Study of Protein-Fluoropolymer Interactions for Passivation of Blood-Contacting Surfaces

Irini Sotiri

A thesis

submitted in partial fulfillment of the

requirements for the degree of

Master of Science in Bioengineering

University of Washington

2018

Committee:

Buddy D. Ratner, Chair

Lara J. Gamble

Program Authorized to Offer Degree:

Bioengineering

University of Washington

Abstract

Study of Protein-Fluoropolymer Interactions for Passivation of Blood-Contacting Surfaces

Irini Sotiri

Chair of the Supervisory Committee:
Buddy D. Ratner
Departments of Bioengineering and Chemical Engineering

While decades of biomaterials research have yielded devices that prolong the lives of cardiovascular disease patients, clinicians still rely on dangerous anticoagulants to ensure their anti-thrombogenicity, and thus lack a truly blood compatible biomaterial. Fluoropolymers have offered improvements in this respect, but studies probing protein tight-binding and platelet response have failed to yield correlations between material properties and clinical performance, preventing the optimization of these promising materials. This work presents a fresh approach to addressing this problem, comparing a subset of fluoropolymers with a wide array of properties. Through principal component regression, ESCA, AFM, and contact angle data were compared to adsorption and retention of human albumin and fibrinogen in a competitive binding setting, and preliminary recommendations for certain property-performance relationships were made. The

methods developed represent a solid foundation for increasing number of parameters and sample size to enable the rational design of better blood compatible fluoropolymers.

TABLE OF CONTENTS

LIST OF FIGURES

LIST OF TABLES

ACKNOWLEDGEMENTS

I am eternally grateful for the support which my mother, dear friends, and lab mates have provided. Their encouragement has inspired me to stay determined in taking on all challenges that graduate school and life has presented.

I would like to thank Dr. Buddy Ratner for this opportunity and helpful discussions, and Dr. Lara Gamble for additional support in thesis development. I would also like to thank Dr. Micah Glaz for assistance with AFM; the David Castner Lab for use of its UV-O cleaner and spin coater; Marvin Mecwan and Kyung-Hoon Kim for assistance with radiolabeling; Winston Ciridon for assistance with plasma deposition; Dr. Wai Pang Chan for confocal microscopy consultation; Bob Scott and the UW Physics Department Instrument Shop for help with SolidWorks modeling and machining of fixture designs; Dr. Ilya Reviakine and Dr. May Speer for suggestions regarding fluorescence microscopy and antibodies; Dr. Dan Graham, Dr. Patrick Heagerty, Dr. Ronit Katz, and Siddharth Rath for statistical analysis advice.

This work was funded by the Center for Dialysis Innovation (CDI). Part of this work was conducted at the Washington Nanofabrication Facility / Molecular Analysis Facility, a National Nanotechnology Coordinated Infrastructure (NNCI) site at the University of Washington, which is supported in part by funds from the Molecular Engineering & Sciences Institute, the Clean Energy Institute, the Washington Research Foundation, the M. J. Murdock Charitable Trust, the National Science Foundation and the National Institutes of Health.

Chapter 1. INTRODUCTION

1.1 History of Fluoropolymers

Fluoropolymers are a class of carbon-based materials with C-F bonds that have pervaded a number of fields since their accidental invention in 1938 at DuPont in the form of Teflon™. Known for their chemical inertness and lubricity, fluoropolymers are used in nonstick cookware, weather-resistant apparel, paint products, electronics, and the automotive and healthcare industries. (1,2) The earliest use of fluoropolymers in medicine was in the late 1940s with the implantation of Teflon™ in dogs, which exhibited little to no foreign body response compared to the other materials studied. (3) In 1967, expanded poly(tetrafluoroethylene) (ePTFE) was invented in Japan, paving the way for the first use of ePTFE in the early 1970s as a venous graft and arterial bypass implant that improved patency rates. (4,5) By 1976, W. L. Gore & Associates, Inc. was commercializing ePTFE as Gore-Tex™, a product which is still a household name today. Since then, many other fluoropolymers have been developed. The global market for fluoropolymers was valued at $6.8 billion in 2017, and is projected to grow to $9.9 billion by 2023, with medical device applications comprising a major part of that growth. (6) The potential for continued impact of fluoropolymers on humanity continues to drive research and development of these materials.

1.2 Chemistry of Fluoropolymers

Fluoropolymers are highly fluorinated thermoplastics with several interesting properties uncommon in other materials, such as hydrocarbons. The C-F bond is the strongest carbon bond,

and has a strengthening effect on adjacent aliphatic bonds that imparts very high chemical resistance and thermal stability. Fluorine itself has a high ionization potential energy and low polarizability, giving fluoropolymers weak intermolecular forces, low interfacial energies, and low refractive indices. The relatively larger atomic radius of fluorine compared to that of carbon also has direct effects on polymer structure, which, combined with the properties above, has important implications for manufacturing. (7)

PTFE is a high-molecular-weight perfluorinated polymer made by radical polymerization of TFE gas. It has a rigid helical chain orientation, containing C-F dipoles distributed axially around the helix, due to the enlarged radius and self-repulsion of fluorine. The rod-like chains result in high bulk solid fractional crystallinity, while the low inter-chain interaction results in slippage that imparts macroscopic lubricity. (7,8) Notably, its high molecular weight and conformational rigidity make PTFE very viscous, while its chemical inertness makes it hard to dissolve, which preclude extrusion and injection molding, (common processes used in manufacturing thermoplastic medical devices). Instead, PTFE parts are often made by compressing and sintering pre-polymerized PTFE granulated powder in a mold at high temperatures (~260°C). (9) These can be shaped as rods, for example, and skived into sheets or films by rolling against a blade, (10) or molded into small-diameter and multi-lumen catheters with high precision. (8)

FEP was made by Dupont in 1956. A perfluorinated copolymer of HFP (C_3F_6) and TFE (C_2F_4), it is made by free radical polymerization of its constituents and has bulky perfluoromethyl groups that create defects which lower crystallinity and melt viscosity. This demands less extreme manufacturing temperatures (~204°C) than pure PTFE, making FEP more preferable for use in medical devices. Partially fluorinated, PVDF has a zig-zag chain

conformation with different C-F dipole alignments along the chain, as opposed to the identical dipole through the zig-zag chain of polyethylene (PE). It is made by radical polymerization of gaseous vinylidene difluoride, then post-processed. It is highly crystalline due to the interpenetration of large CF_2 groups with small CH groups on adjacent chains. PVDF is a unique fluoropolymer because it has a lower melt processing temperature than PTFE, can be dissolved in various solvents, and has piezoelectric properties that result in solid state structures with chemical and thermal stability - all useful aspects in designing medical devices. (8)

Until now, only bulk manufacturing methods have been discussed. However, due to the costs associated with these methods, surface fluorination of cheaper bulk materials is an attractive option to obtain coatings that retain the hydrophobicity, lubricity, and chemical resistance that is so desirable in fluoropolymers. Dissolving monomers in solution and spin casting is one easy coating method that can be tuned to create thin film coatings. (11) Another more versatile way is plasma deposition, a surface modification technique in which a monomer gas is flowed through a pressure-controlled chamber and ionized by the application of voltage between two electrodes. After a critical voltage is reached, the gas glows with a characteristic color. Placement of samples in the deposition chamber results in a highly crosslinked, strongly-adhered rigid coating that is of similar but not identical molecular structure to the monomer. This is because the ionization results in a combination of free radicals and monomer fragments polymerizing somewhat randomly on the substrate. Moreover, the distribution of chemical groups can be altered by placement of substrates in the glow, upstream of the glow, or downstream of the glow. Fluorocarbons such as TFE and HFP have been plasma deposited via radio frequency glow deposition (RFGD) on substrates with varied geometry to change their hydrophobicity, and have resulted in favorable biocompatibility properties. (11–13)

1.3 Fluoropolymers in Medical Devices

As mentioned in Section 1.1, fluoropolymers saw early use in and continue to be developed for healthcare, with a majority of applications in medical devices. The most common fluoropolymers are PTFE, polyvinylidene fluoride (PVDF), hexafluoropropylene (HFP), and fluorinated ethylene propylene (FEP), the chemical structures of which are shown in Figure 1. Given their chemical and thermal stability, fluoropolymers have been made into a variety of forms - solids, liquids, gasses, thin films, surface coatings, gels - which have resulted in their widespread therapeutic use.

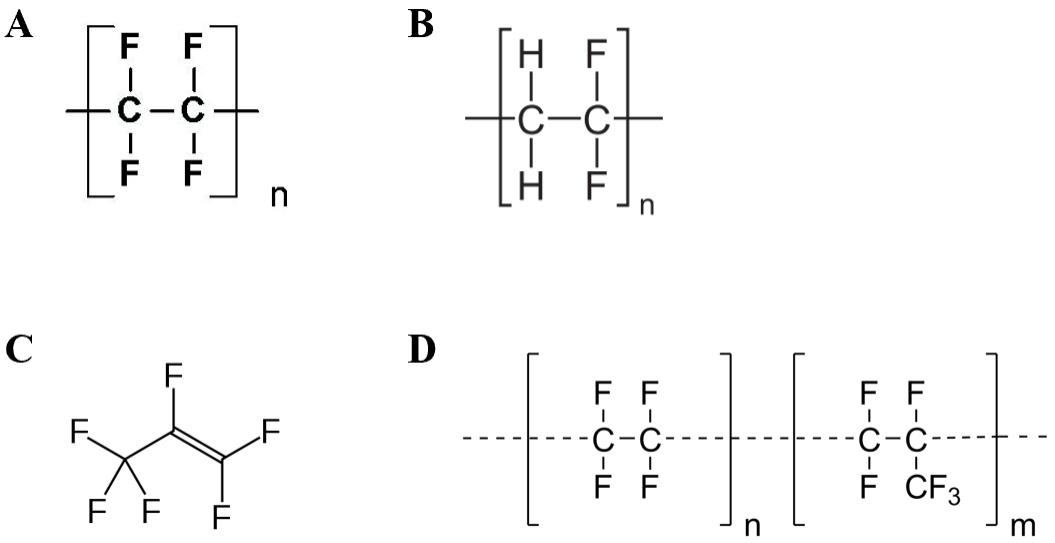

Figure 1.1 Chemical structures of common fluoropolymer monomers. (A) PTFE, (B) PVDF, (C) HFP, (D) FEP.

Teflon™ (PTFE) is used in medical tubing, multi-lumen and guiding catheters, and sutures. (14) Gore-Tex™ (ePTFE) is used in vascular grafts, (15) hernia meshes, (16) and ligament replacement. (17) PVDF is used for protein blotting/separation membranes in the

biotech industry. (18) Perfluorinated liquids were once applied as blood (19) and ocular vitreous (20) substitutes, while analogous gels have been used in contact lens construction, due to their high oxygen permeability. (21) Plasma deposition of fluoropolymers has been used for creating anti-fouling contact lens coatings, and offers an easy way to obtain a fluorinated surface on varied geometries without the added cost of bulk fluoropolymers. (8) The copolymer PVDF-HFP has recently been used to coat drug-eluting cardiovascular stents such as the XIENCE V® DES coronary stent (Abbott Vascular). (11,22) These examples clearly illustrate the positive impact of fluoropolymers on healthcare.

Chapter 2. BACKGROUND

2.1 THE PROBLEM OF BIOCOMPATIBILITY

Heart disease and stroke are the leading causes of death worldwide. Though regenerative therapies will someday address these problems, for the foreseeable future, millions of cardiovascular devices will be implanted in humans each year as interventions after heart attack and other conditions. (23) Surgical procedures for implanting medical devices come with uncontrolled interaction of proteins with device surfaces that negatively impacts performance. The introduction of a foreign surface into the body triggers the extrinsic (platelet) pathway in the coagulation cascade. First, a layer of serum proteins adsorbs whose composition dictates interactions with platelets (including aggregation) and inflammatory cells. This can result in platelet activation, which can lead to thrombotic complications including emboli. (24) The anticoagulants prescribed to prevent such events must be taken for life despite the dangers associated with their long-term use, such as increased risk of hemorrhage, and impaired kidney and liver function. (25)

While researchers in tissue engineering, regenerative medicine, and drug delivery are progressing in the effort to repair the body naturally, bringing such research to market is an arduous task. (24) Alternatively, materials-based solutions have faster development cycles and are already in market, as evidenced in Section 1.3 and by low-fouling polymeric coatings on some blood-contacting devices. (26) Still, no such coatings are truly biocompatible; (27) they either elute or require the administration of anticoagulants, and can still lead to thrombotic and embolic complications. Scientists and engineers still need to develop materials that are more blood compatible – that is, materials that function with minimal or no anticoagulation, and do not generate clots or emboli over periods of weeks. (25) However, doing so requires a better

understanding of the relationships between material properties and performance than is currently available.

Many attempts have been made since the 1970s to discover correlations between material properties and clinical results, but all have been plagued by most, if not all, of the following issues: insufficient sample size, material/device complexity, intricate/convoluted biological response, and insufficient consideration of multivariate effects. (8,28) While a lot of progress was made, these challenges tempered the enthusiasm and expectations of the biomaterials community for solving the biocompatibility problem with a materials approach, and saw the rise of the pharmaceutical patch fixes (e.g. anticoagulants) we know today in the fields of tissue engineering and regenerative medicine. Perhaps these will succeed, or perhaps a combined cell and materials approach will be necessary. Regardless, it is clear that a fresh, stripped-down approach is needed to develop property-performance recommendations for designing materials that can solve the blood compatibility problem. To mitigate the seemingly unavoidable pitfalls of past attempts mentioned above, this fresh approach should (1) span a range of chemistries and other properties without using drastically different materials that might overcomplicate and confound interpretation of results, (2) begin with a logically selected foundation of parameters, and expand them iteratively to control complexity, (3) utilize multivariate factor analysis methods, and (4) have high sample size to increase confidence in the resulting recommendations.

2.2 Theoretical Background on Blood Compatibility

The clotting process is complex, comprising intrinsic and extrinsic pathways that ultimately converge. This research is relevant to the extrinsic pathway, which dominates after blood vessel injury by foreign bodies. Upon blood contact, a layer of serum proteins adsorbs whose composition dictates interactions with platelets (including aggregation) and inflammatory cells. A cascade ensues in which fibrinogen (Fbg) converts to fibrin and platelets activate, which can lead to thrombotic complications. (29) Subsequent tissue repair involves clot-dissolving fibrinolysis that can create emboli. (8) An important note is that in initial protein deposition, albumin (Alb), the most abundant plasma protein, adsorbs first but can be displaced by fibrinogen due to its higher surface affinity and molecular weight due to the Vroman effect. (30) Studies have shown Fbg to be a key player in platelet adhesion and activation, (31) so it stands that materials that resist Fbg adsorption could mitigate thrombotic fouling.

One suggested strategy is to engineer a surface that tightly binds Alb so that it cannot readily be displaced, passivating the surface due to Alb's relative inertness. (8,32–34) Certain fluoropolymers have been shown to readily bind serum proteins, such as Alb, non-specifically and very tightly, (8,11,35–37) and are valued in industry as vascular implant materials that exhibit low thrombogenicity and inflammatory response. (8,11) Plasma deposited TFE has been shown to tightly bind albumin, (35) and although this gas is not sold anymore due to the environmental effects of its productions, HFP is a close substitute with the same fluorine to carbon ratio. PVDF has been shown to prefer fibrinogen and fibronectin, which is a cell-adhesive protein, (38) while PTFE was observed to bind high amounts of fibrinogen, fibronectin, and albumin. (8) The concept of passivation by albumin tight-binding has been explored on non-

fluorinated surfaces as well, and found albumin preference to be inversely related to platelet activation. (34)

However, studies have shown that it is also possible that a denatured layer of fibrinogen whose platelet-binding epitopes are inaccessible could also serve as a passivating layer. (29,39) Finally, since protein adsorption dictates subsequent cellular response, and platelets are cells central to thrombogenesis, we must note the published idea that platelet membranes themselves are very inert, once the platelets release their granules and fully spread onto a surface. This suggests platelet spreading as an additional surface passivation strategy for achieving biocompatibility in blood-contacting medical devices. (26,30) In summary, while much effort has been invested in understanding surface protein-cell interactions, including on fluoropolymers, there is no definite understanding as to why some fluoropolymers clinically outperform others, or why different fluoropolymers bind preferentially to different proteins. Conjecture has been made to some extent on individual fluoropolymer surfaces, but a comprehensive comparison of a larger set of medically relevant fluoropolymers has not been published.

2.3 Scope of this Study

This thesis is the first part of a multifaceted project aimed at designing a fluoropolymer coating that, utilizing one of the surface passivation strategies mentioned in Section 2.2, functions in contact with blood with minimal or no anticoagulation, and does not generate clots or emboli over periods of weeks. The first clinical application of this coating will be in a portable hemodialyzer in development at the Center for Dialysis Innovation (CDI). While the overall project represents a massive undertaking comprising the efforts of a team of researchers, the

work described herein lays the foundational knowledge and experimental methods needed to launch and complement other parts of the project (described in Section 8.2 and Appendices).

This work aims to uncover why albumin and fibrinogen adsorb more on particular fluoropolymer surfaces than others. The first hypothesis is that the chemical composition of a fluoropolymer determines its protein affinity, with CH and CF_2 content playing important roles. The latter idea is based on the use of PVDF and PVDF-containing materials in performing well clinically and showing interesting results in the initial experiments. (22) The second hypothesis is that differences in the physical structure of a fluoropolymer determine its protein affinity, namely through roughness and manufacturing method. The third hypothesis is that surface energy determines protein affinity. This idea has had some support in the past, but is still debated. (8)

While there are many publications showing protein adsorption and cell adhesion on fluorinated surfaces, they were primarily done in the 1980s-90s and used one or two fluoropolymers as a subset of a set of materials containing no fluorine. The work herein is a wider multivariate study comparing a larger number of only fluorinated surfaces with the goal of finally discovering what aspects of the fluorination impact protein adsorption. To mitigate the property-performance pitfalls of past biomaterials research described Section 2.1, eight fluoropolymers were studied to provide a range of chemical group distributions, contact angle, roughness, and manufacturing method - all termed properties or “predictors.” The performance of “outcome” variables were adsorbed albumin and fibrinogen, retained albumin and fibrinogen, % retention of each protein, and ratios of adsorbed Alb:Fbg and retained Alb:Fbg.

Electron spectroscopy for chemical analysis (ESCA) was used to determined surface chemical composition and CF group content. A goniometer was used for obtaining static water

contact angles. Atomic force microscopy (AFM) was used to measure RMS roughness. Radiolabeling was used to measure albumin and fibrinogen adsorption and retention in a competitive binding setting. While discussed only in the Appendices, scanning electron and confocal microscopy were also used to optimize protocols for platelet morphology analysis. Multivariate factor analysis using principal component regression resulted in the suggestion of property-performance relationships, and recommendations of properties for a given desired protein response.

Chapter 3. EXPERIMENTAL

3.1 MATERIALS

All water used in experiments was ultrapure (Type 1), deionized to a resistivity of 18.2 MΩ•cm at 25°C using the Synergy® Water Purification System from MilliporeSigma. The FEP film used was purchased from ALZA Corporation, the PTFE film from Jensen Inert Products (#15076-P065005), and the PE film was a standard provided by the National Heart and Lung Institute. The PVDF (Aldrich Chemistry, #427152) and PVDF-HFP (Aldrich Chemistry, #427160) were both dissolved in anhydrous dimethylformamide (DMF) from EMD Millipore Corporation (#DX1730-6). The albumin from human serum was purchased from Sigma-Aldrich (#A8763) and the fibrinogen from human serum was purchased from Sigma-Aldrich (#F3879). The same lot numbers were used for all experiments. Sodium dodecyl sulfate (SDS) was purchased from Bio-Rad (#1610302). Isopanasol concentrate used in diluted cleaning solutions was purchased from CR Callen LLC, while Micro90 cleaning diluent was purchased from International Products Corporation (#M-9050-12). Borosilicate glass coverslips were purchased from Knittel Glass (G401-08). Hexafluoropropylene (HFP) gas was purchased from Synquest Laboratories (CAS #116-15-4), and ultra-high purity methane gas was purchased from Matheson (#UN1971).

.

3.2 SAMPLE PREPARATION

3.2.1 *Preparation of Commercial Fluoropolymers*

All glassware and tweezers were cleaned prior to use by soaking overnight in a 2%(v/v) solution of Micro90 and water, then rinsing four times with water and allowing to air dry. Prior to

cleaning the commercial fluoropolymers (PE, PTFE, and FEP), circular discs were extracted from the bulk film using a biopsy punch of 8mm diameter. The samples were then secured in a custom-made stainless steel holder, and sonicated for five minutes in a solution of ratio 1:64 with isopanasol and water. The cleaning solution was replaced with water four times, each time sonicating for five minutes, followed by a final three-minute soak in methanol. Samples were dried with nitrogen gas and stored in nitrogen back-filled petri dishes that were sealed with parafilm to maintain surface cleanliness.

It is important to note that two types of skived PTFE were used. In addition to samples simply punched out of the bulk skived PTFE film, samples punched from stretched skived PTFE were also used. The goal of stretching was to plastically deform the PTFE so as to alter the orientation of the polymer chains and their CF_2 groups. A load-extension curve (Figure 3.1) of dry skived PTFE was generated at room temperature in BlueHill software by an Instron benchtop tensile tester (#5543Q3491), using the ASTM D882 Standard Test Method for Tensile Properties of Thin Plastic Sheeting (ASTM) as a guideline for the following test parameters: 25x150 mm strips were cut along the skiving direction and secured with 100 mm grip separation, then stretched at 25 mm/min. As shown in Figure 3.1, this test determined the maximum elongation for the skived PTFE to be ~55%. Based on this, and to ensure a majority plastic deformation without fracture, 40% elongation was chosen for all stretched skived PTFE used in experiments, with an additional static minute allowed for creep at the 40% elongation. Stretching was performed 24 hrs prior to sample use, with punching done from the center of the stretched strip.

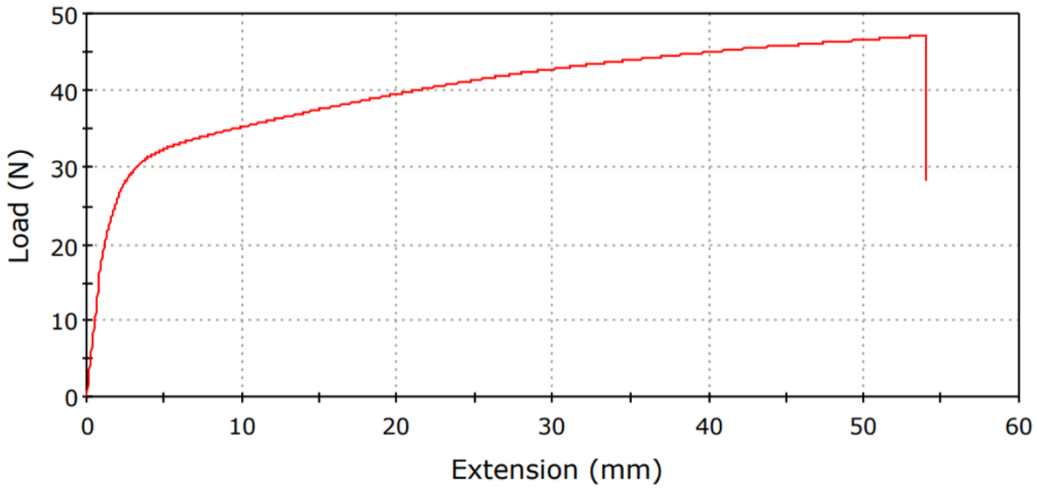

Figure 3.1. Sample result of tensile tests used to decide stretching extent for stretched skived PTFE.

3.2.2 *Optimization and Preparation of Spin-Coated Fluoropolymers*

A spin coater from Specialty Coating Systems, Inc. (model P6700) was used for creating thin PVDF and PVDF-HFP films. Given the difficulty of dissolving FPs, multiple solvents, temperatures, and concentrations were tested to determine the best choices for dissolving both PVDF and PVDF-HFP. Acetone and N-Methyl-2-pyrrolidone did not dissolve PVDF even at 40°C. The final solvent was chosen to be anhydrous dimethylformamide (DMF) at a 3% (w/w). Other parameters optimized to prevent vapor-induced phase separation during spin coating and ensure total sample coverage were: substrate (borosilicate glass coverslip, EMA-silanized glass coverslip, gold-coated glass coverslip), substrate prep (UV-O cleaning), droplet volume, drop method, spin speed, spin duration, ramping times, and chamber humidity. Visual examination and ESCA were used to verify results. The optimized combination used in experiments had the following parameters. The substrate was a gold-coated borosilicate glass coverslip with a titanium adhesion layer, UV-O treated for 1 minute prior to spin-casting, while the spin coater chamber was prefilled with nitrogen gas to minimize humidity. A droplet of 18 µL polymer

solution was micropipetted onto the mounted substrate, and a nitrogen nozzle moved one inch directly above the substrate flowing gas at 50 kPa. The sample was spun for 2 minutes at 2000 rpm, with 5 s ramp-up and ramp-down times, after which it was allowed to air dry overnight in a nitrogen-backfilled petri dish inside a fume hood. Figure 3.2 shows the improvement in the quality of the spun coatings as parameters were increasingly optimized.

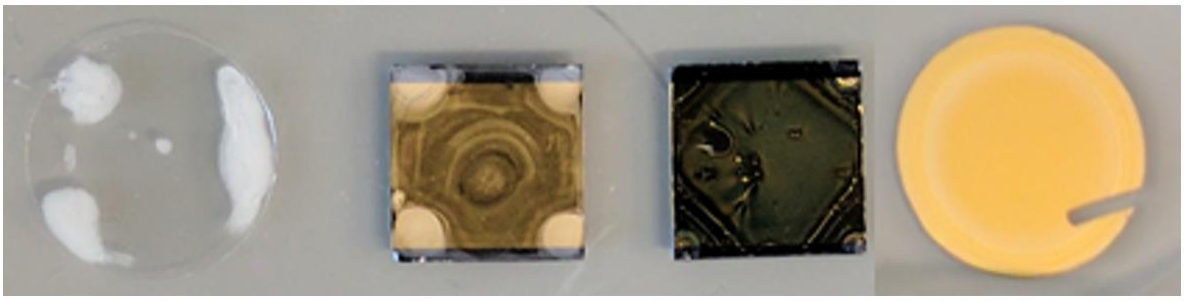

Figure 3.2 Improvement in spin-cast coating quality throughout optimization (left to right).

Delamination testing was essential to ensure stability of the coating, and was conducted by soaking a coated sample overnight in water on an orbital shaker, drying then comparing ESCA spectra to a non-washed control. All coatings used in experiments passed delamination tests. Additionally, a custom aluminum fixture was designed to allow for double-sided electron beam evaporation of the titanium/gold coatings. A schematic of this with explanation of its motivation and operation is shown in Appendix A.

3.2.3 *Preparation of Plasma-Deposited Fluoropolymers*

Plasma deposited FPs utilized a custom-built radio frequency-powered glow deposition (RFGD) chamber with capacitive coupling that allows for robust control over pressure, flow rate, supplied power, and sample placement relative to plasma glow. Glass coverslips were first cleaned with

isopanasol using the procedure outlined in Section 3.2.1, then arranged upstream and downstream of the glow region in the chamber according to Figure 3.3. Next, samples were cleaned by argon etching for 5 minutes at 40 W, 200 mT, and 62.1 sccm. A methane adhesion layer was deposited for 5 minutes at 80 W, 150 mT, and 1.5 sccm, followed by an HFP adhesion layer for 1 minute at 60 W, 150 mT, and 10 sccm. Then, the desired HFP coating was deposited for 20 minutes at 20 W, 150 mT, and 10 sccm, followed by a 5-minute quenching step with no power. The coatings were allowed to settle under vacuum before the samples were flipped over and the entire process repeated to coat the second side. A delamination test was run as described in Section 3.2.2, confirming the coating stability.

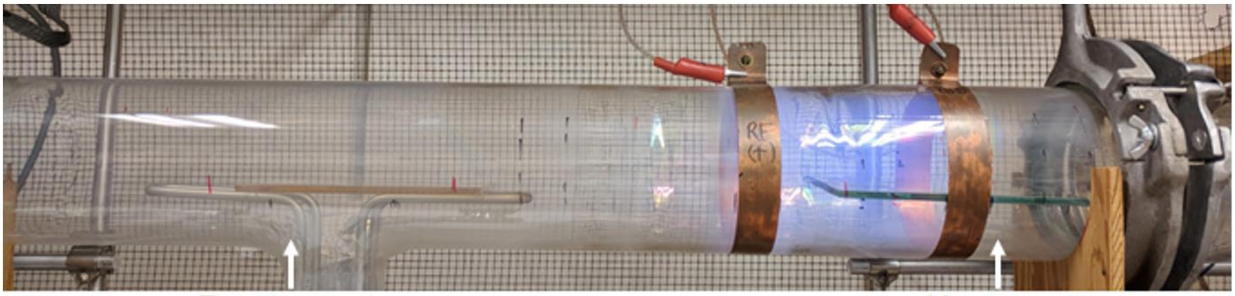

Figure 3.3 Sample placement in RFGD chamber relative to plasma glow.

3.3 Sample Characterization

3.3.1 *ESCA Analysis*

The chemical composition of every coating was characterized by electron spectroscopy for chemical analysis (ESCA) at the National ESCA and Surface Analysis Center for Biomedical Problems (NESAC/BIO, University of Washington, Seattle). For spin-cast and plasma deposited coatings, high-resolution ESCA spectra of carbon (C1s), and oxygen were compared between

samples subjected to the delamination test described in section 3.2.1 and their respective controls to confirm coating stability. A Surface Science Instruments S-Probe, with a monochromatic Al Kα1,2 x-ray source and 0° take-off angle yielded data reflecting the composition of the outermost 10 nm of each surface. A metal mesh was placed just above the samples to prevent surface charging during analysis. Compositional survey scans (0–1000 eV) were acquired using an analyzer pass energy of 150 eV and an x-ray spot size of 800 μm. High-resolution spectra were acquired at a pass energy of 50 eV and resolved into individual Gaussian peaks using a least-squares fitting routine in Hawk 7 Analysis software. All binding energies (BE) were referenced to the lowest resolved C1s peak BE, the hydrocarbon peak (CH) at 285.0 eV. Compositions are reported as the average of the collected spots for one type of material, and presented as atomic percent (n=6, three spots per two samples).

3.3.2 *AFM Analysis*

An Asylum Research CypherES was used to acquire atomic force microscopy images. The samples were taped to a magnetic puck, and a 150 kHz cantilever purchased from BudgetSensors was used in tapping mode to collect the topographic data. A survey of multiple regions was conducted, and representative spots were chosen. All images were captured away from sample edges to avoid edge irregularities, and analyzed using Gwyddion data analysis for statistical analysis (n=3, one representative spot measured per three samples).

3.3.3 *Contact Angle Analysis*

Static water contact angle was measured on each polymer using the sessile drop technique with a goniometer. An FTÅ200 video system (First Ten Angstroms, Inc., Portsmouth, VA) was used, complete with a high-resolution camera and zoom microscope, computer controlled vertical

syringe pump and lighting, adjustable specimen stage, and built-in analysis software. Clean surfaces stored under nitrogen were placed on the stage, a 5 μL droplet was deposited onto the surface (towards the center to avoid edge effects), and an image was captured. Automatic angle calculation was performed after first defining surface and droplet edges manually. Values are reported as the average of the angles measured for one type of material, with one spot measured per three samples (n=3).

3.4 Protein Adsorption Assay

Protein adsorption and retention was measured under competitive binding conditions of human albumin and fibrinogen using radiolabeling. The ICl method, developed by Helmkamp et al. (40) and modified by Horbett (41) labels the proteins with ^{125}ICl (PerkinsElmer, Waltham, MA) one at a time, and the experiment is conducted twice to obtain measurements for each protein. A 2:1 ICl to protein molar ratio was used for labeling fibrinogen, while a 3:1 ICl to protein molar ratio was used for labeling albumin. Unbound ^{125}I was separated from the labeled protein by two passes through desalting chromatography columns (EconoPac 10DG, BioRad, Hercules, CA) and collected in successive cuvettes. Successful isolation of labeled protein was confirmed by monitoring cuvette readouts from a Cobra II γ-counter. The purified radiolabeled protein was stored at 20°C and used the following day to minimize loss of activity. Samples were submerged in degassed CPBSzI buffer for 2 hrs at room temperature to equilibrate, and a fresh binary protein solution (0.6 mg/ml albumin and 0.06 mg/ml fibrinogen) was made. A small amount of high-activity ^{125}I stock, not enough to significantly change the protein concentration, was added to reach a specific activity of no less than 50 cpm/ng. The hot binary protein solution was then added to the samples soaking in CPBSzI at an equivalent volume, so as to reach a final protein concentration consistent with 1% plasma (0.3 mg/ml albumin and 0.03 mg/ml fibrinogen). Samples were then

incubated for 2 hrs at room temperature, and bulk protein was rinsed away three times with fresh CPBSzI using a custom continuous flow setup.

After rinsing, samples were placed in tubes and their radioactivity measured with a γ-counter, along with hot protein stock controls. The amount of labeled protein adsorbed per sample was calculated from the bound ^{125}I using the specific activities of the protein and the surface area of both sides of the sample, with corrections for background radioactivity. To measure retention of labeled protein, the samples were then incubated in 2% SDS for 24 hrs, then rinsed with CPBSzI under continuous flow for 3 s. Their radioactivity was measured again in new tubes using the γ-counter, with saved hot protein stock controls to account for decay in calculation of remaining adsorbed (i.e. retained) protein.

3.5 Statistical Analysis

For the sake of simplicity, all ESCA, contact angle, and AFM data are referred to as predictors, and all protein response variables are referred to as outcomes. For intra-experiment comparisons, unpaired t-tests were used to compare the means of all material groups to that of PVDF, which appears to have the most interesting behavior. ANOVA with Sidak correction was used for multiple comparisons. The Pearson correlation coefficient was calculated for each combination of predictor to assess multicollinearity, and for combinations of predictors and outcomes. To decrease dimensionality and effects of predictor collinearity, principal component analysis (PCA) was performed on the predictors using Spectragui software. The outcomes were then regressed on the scores of the resulting principal components (PCs). The loadings of the PCs whose coefficients of determination were significant ($p < 0.1$) were compared with the scores of their respective PCs. The relevant scores were plotted against the outcomes, and the sign (+/-) of the scores that corresponded with higher values in the outcomes was used to choose the loadings most important

to the outcome. This method provided a direct way to extract which physical and chemical parameters corresponded the most with the given outcome variable, without the influence of multicollinearity in predictors.

Chapter 4. ESCA ANALYSIS

4.1 PURPOSE

Electron spectroscopy for chemical analysis (ESCA) is a non-destructive surface analysis technique that provides information about the chemical composition and molecular environment (e.g. oxidation state) of approximately the outermost 10 nm of a sample. Also known as X-ray photoelectron spectroscopy (XPS), ESCA utilizes the photoelectric effect, where a surface bombarded by an X-ray source emits electrons whose kinetic energies can be measured and correspond to specific elements and atomic orbitals. This results in spectra with peaks whose areas and binding energies can be used to calculate atomic percentage of an element (usually from survey spectra ranging 0–1000 eV) and carbon-bound chemical group (from high-resolution C1s spectrum). ESCA was utilized as the primary characterization tool in this work, to confirm both surface identity (and successful deposition for non-commercial materials) and stability in the face of delamination testing described in section 3.2.1. It yielded a number of useful predictors to be compared with protein binding behavior: %C, %F, %CF, $\%CF_2$, $\%CF_3$, and parameters calculated from these readouts such as F:C ratio and degree of fluorination. The materials analyzed were the non-fluorinated control polyethylene (PE), fluorinated ethylene propylene (FEP), polytetrafluoroethylene (PTFE), polyvinylidene fluoride (PVDF), Poly(vinylidene fluoride-co-hexafluoropropylene) (PVDF-HFP), and hexafluoropropylene (HFP). These were chosen to provide a range of fluorine group content and manufacturing method, which is necessary to determining property-performance relationships. This is summarized below in Table 4.1.

Table 4.1 Summary of materials studied.

Polymer	Manufacturing Method	Chemical Group Content
PE	Commercial	CH
FEP	Commercial	CF, CF_2, CF_3
PTFE	Commercial: skived, stretched	CF_2
HFP (upstream)	RFGD (upstream of glow)	CH, CF, CF_2, CF_3
HFP (downstream)	RFGD (downstream of glow)	CH, CF, CF_2, CF_3
PVDF	Spin coated	CH, CF_2
PVDF-HFP	Spin coated	CH, CF, CF_2, CF_3

4.2 Results and Discussion

4.2.1 *Spectral Analysis*

The following spectra are representative high-resolution C1s scans from each material studied. Results discussed below do not include spectra from samples that underwent delamination testing because the final samples used all passed the test and had identical spectra post-testing. In this case, identical refers to no change in carbon and fluorine content, no appearance of oxygen, and similar peak envelopes in the C1s spectra. Where appropriate, peak envelopes were resolved into individual Gaussian peaks using a least-squares fitting routine in Hawk 7 Analysis software. All peaks were confined to an 80% Gaussian shape and had their FWHMs constrained to be the same. All binding energies (BE) were referenced to the lowest resolved C1s peak BE, the hydrocarbon peak (CH) at 285.0 eV, as is standard practice.

Figure 4.1 shows the C1s spectrum of polyethylene, a high-purity calibration standard whose production was sponsored by the National Heart and Lung Institute in the mid-late 1900s for biological testing and physicochemical characterization of biomedical polymers. Unfortunately, manufacturing information was unavailable for this material. However, it is known that high-density polyethylene (HDPE) is the type of PE most used in medical settings,

and it can be manufactured in three ways. All involve addition polymerization kinetics with catalysis of purified ethylene, but may be done in slurry, solution, or gaseous processes. Regardless, hydrogen is mixed in to control polymer chain length, and the resulting product is a powder which is then extruded to increase chain linearity (and thus intermolecular forces), then cut into granules for further processing depending on the desired final form. The PE studied herein came in sheet-form, so it was likely either heat-pressed or extruded/rolled. (42) The ESCA spectra show an expected 100% hydrocarbon content.

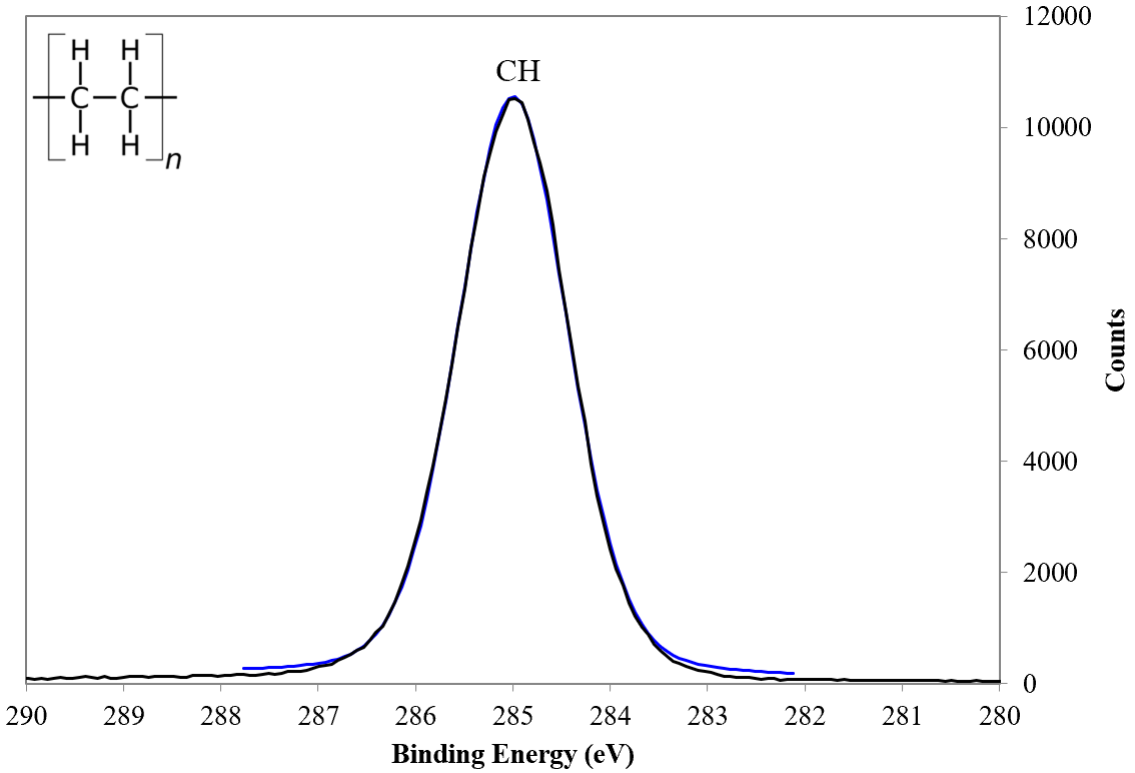

Figure 4.1 C1s spectrum of PE with monomer inset.

Figure 4.2 shows the C1s spectrum of FEP, which is a copolymer of TFE and HFP made from their free radical polymerization and post-processing into sheet form. The peaks identified match reports in literature, (43) with the C1s envelope consisting of 8.4 ± 7.6 % CH, 2.9 ± 2.6 % CF, 75.2 ± 8.0 % CF_2, and 9.4 ± 8.2 % CF_3. While this film seemed to have the highest variation

in composition across its surface of the materials studied (possibly due to manufacturing), the overall elemental content obtained from ESCA survey spectra was 36.6 ± 4.9 % C and 61.9 ± 6.5 % F, which matches the F:C ratio expected from literature. (43)

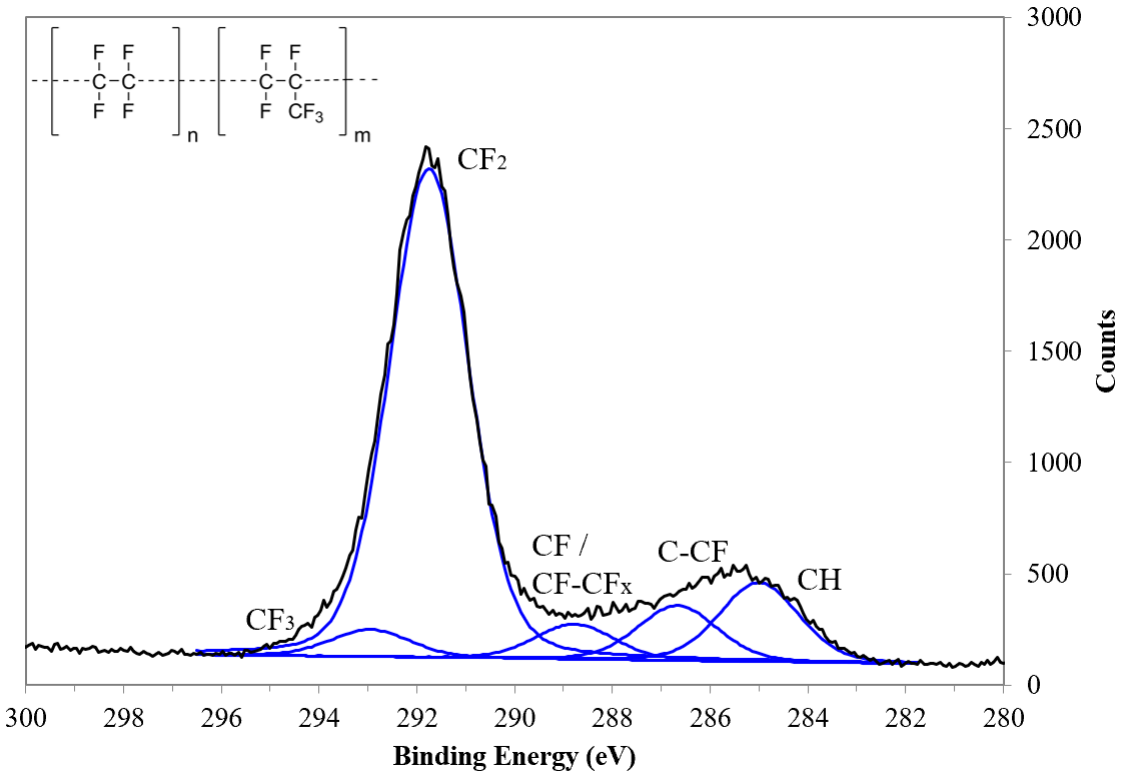

Figure 4.2 C1s spectrum of FEP with monomer inset.

Figure 4.3 shows the C1s spectrum of PTFE, which should contain purely CF_2. This was the case with most PTFE samples analyzed in ESCA, with the average CF_2 content being 98.4 ± 2.6 %, and the average CH content being 1.6 ± 2.6%. Both the skived and the stretched skived PTFE samples naturally have the same spectra. The overall elemental content obtained from ESCA survey spectra was 32.9 ± 1.9 % C and 68.0 ± 1.9 % F, which is very close to the theoretically expected F:C ratio of 2.

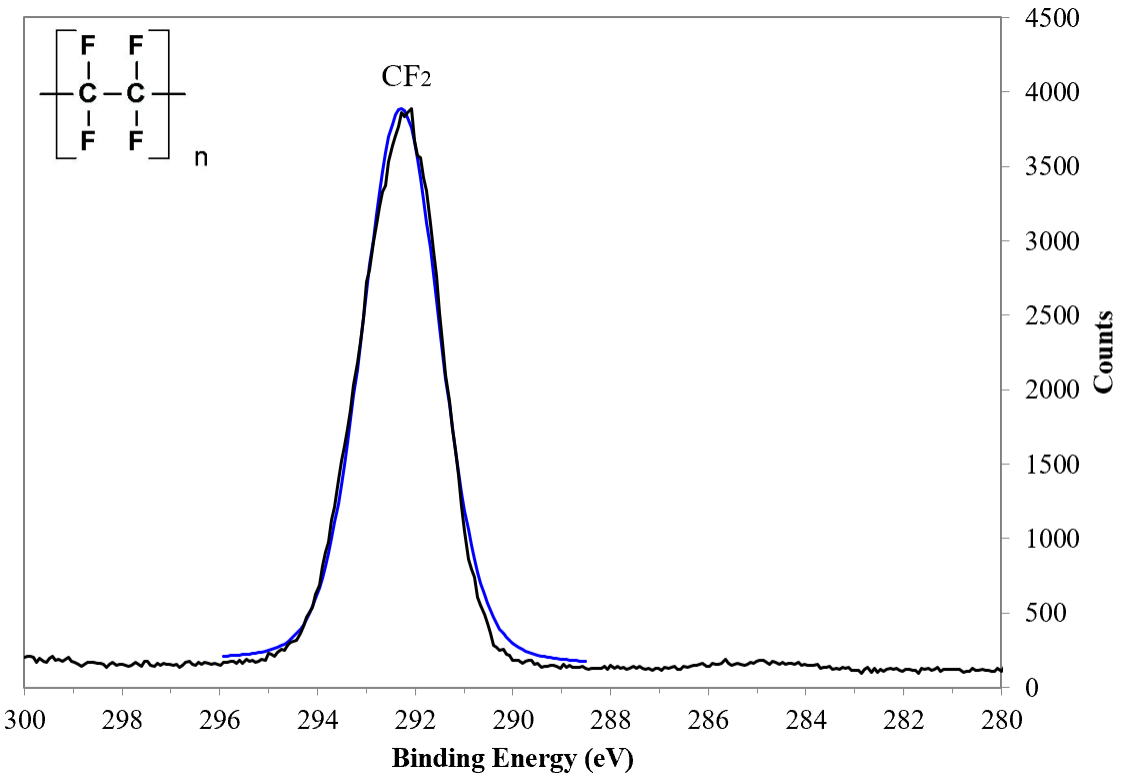

Figure 4.3 C1s spectrum of PTFE with monomer inset.

Figure 4.4 shows the C1s spectrum of PVDF, which was made from pellets dissolved in DMF and spin-coated onto gold-coated glass coverslips. No remnants of DMF are apparent in the ESCA spectra, meaning all solvent evaporated successfully and yielded a pure coating. No gold was visible in the survey spectrum, meaning the coating was thicker than 10 nm. The overall elemental content obtained from ESCA survey spectra was 48.7 ± 1.4 % C and 51.2 ± 1.4 % F, which is very close to the theoretically expected F:C ratio of 1. Additionally, the C1s envelope consists of 49.7 ± 0.1 % CH, 50.3 ± 0.1 % CF, 75.2 ± 8.0 % CF_2, demonstrating the high reproducibility of the coating method.

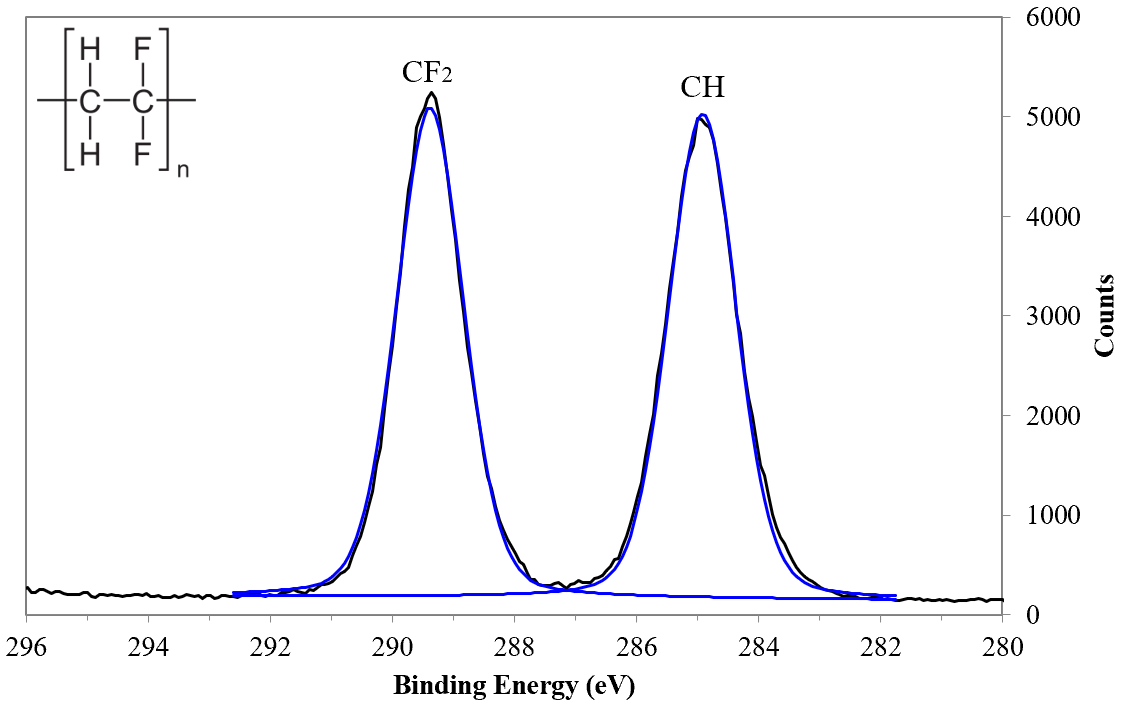

Figure 4.4 C1s spectrum of PVDF with monomer inset.

Figure 4.5 shows the C1s spectrum of PVDF-HFP, which was also made from pellets dissolved in DMF and spin-coated onto gold-coated glass coverslips. No remnants of DMF or gold are apparent in this ESCA spectrum either, suggesting another pure coating thicker than 10 nm. The overall elemental content obtained from ESCA survey spectra was 47.9 ± 1.4 % C and 52.1 ± 1.4 % F, which is very close to the theoretically expected F:C ratio of 1. Additionally, the C1s envelope consists of 45.6 ± 0.4 % CH, 2.0 ± 0.1 % CF, 49.0 ± 0.3 % CF_2, and 3.4 ± 0.1 % CF_3, again demonstrating the high reproducibility of the coating method. This spectra is also similar to reports in literature. (44)

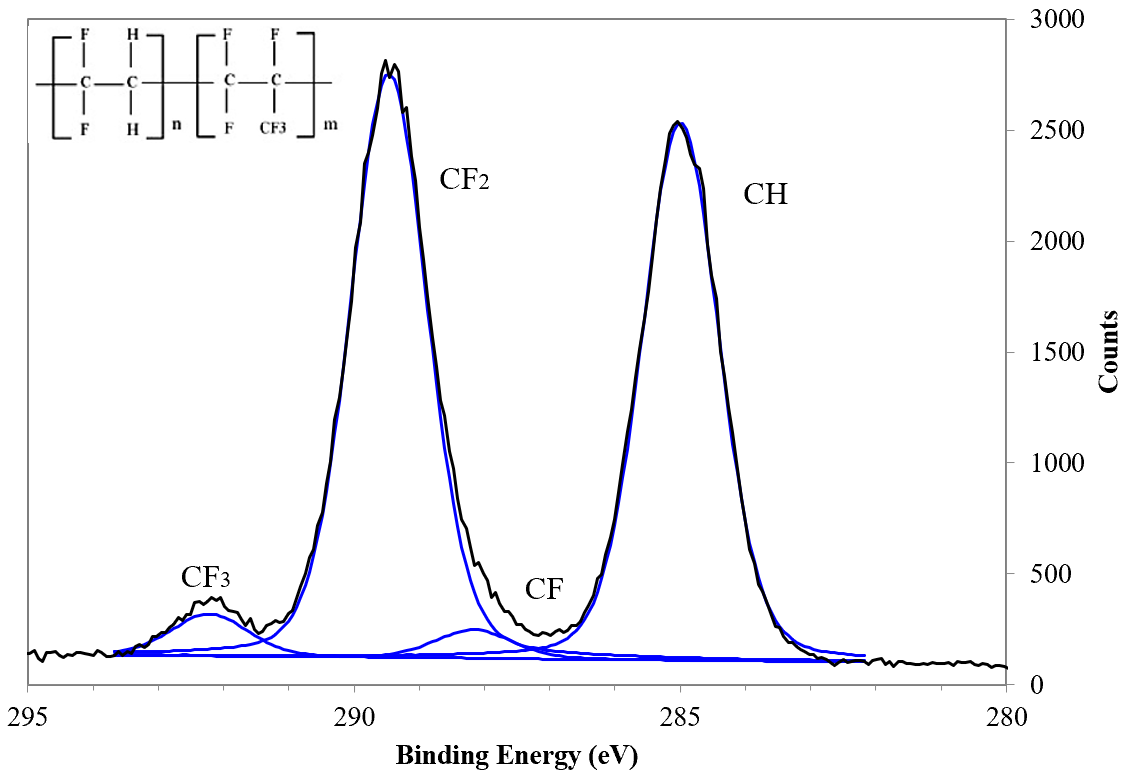

Figure 4.5 C1s spectrum of PVDF-HFP with monomer inset.

Figure 4.6 and 4.7 show the C1s spectra of HFP, deposited ~3 cm upstream and ~ 28 cm downstream, respectively, of the plasma glow in an RFGD chamber (as shown in Figure 3.3). These positions were chosen due to literature demonstrating the ability to control CF group distribution through adjustment of power, flow rate, and sample position relative to the glow (Garrison, 1999; Shard, 1992). In both cases, the presence of C-CF groups, which are not part of the initial monomer, indicate that polymerization is occurring through molecular rearrangement and the fluorine removal from a monomer molecule allowing for reactions with other nearby fragments. The overall elemental content obtained from ESCA survey spectra for HFP (upstream) was 42.1 ± 0.3 % C and 57.9 ± 0.3 % F, and the C1s spectrum is in agreement with the literature, (45,46) The C1s envelope for HFP (upstream) consists of 4.5 ± 1.1 % CH, 20.1 ±

0.8 % CF, 27.0 ± 1.4 % CF_2, and 25.8 ± 0.3 % CF_3. The C-CF content is not considered a relevant predictor, and thus not reported. The overall elemental content obtained from ESCA survey spectra for HFP (downstream) was 46.1 ± 0.3 % C and 48.4 ± 0.4 % F. The C1s envelope for HFP (downstream) consists of 3.6 ± 2.6 % CH, 20.5 ± 1.0 % CF, 22.4 ± 3.1 % CF_2, and 11.1 ± 3.8 % CF_3. Overall, it is apparent that CF_2 and CF_3 content decrease with downstream deposition, and that sufficiently different HFP coatings have been simultaneously deposited.

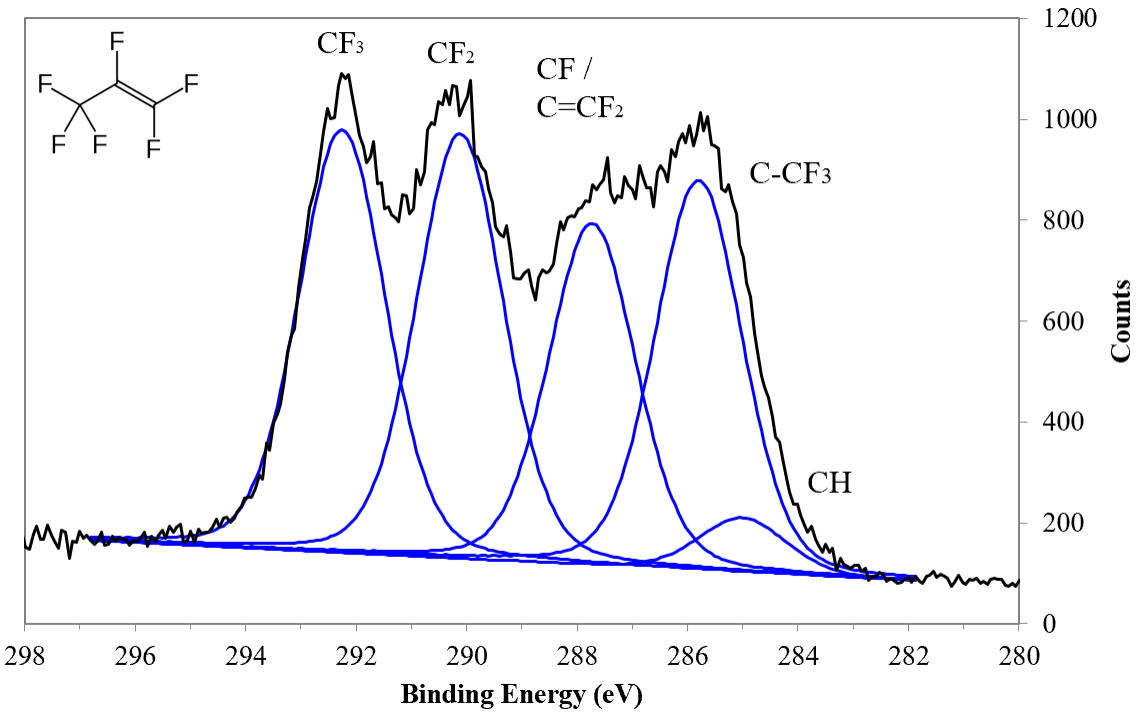

Figure 4.6 C1s spectrum of HFP (upstream) with monomer inset.

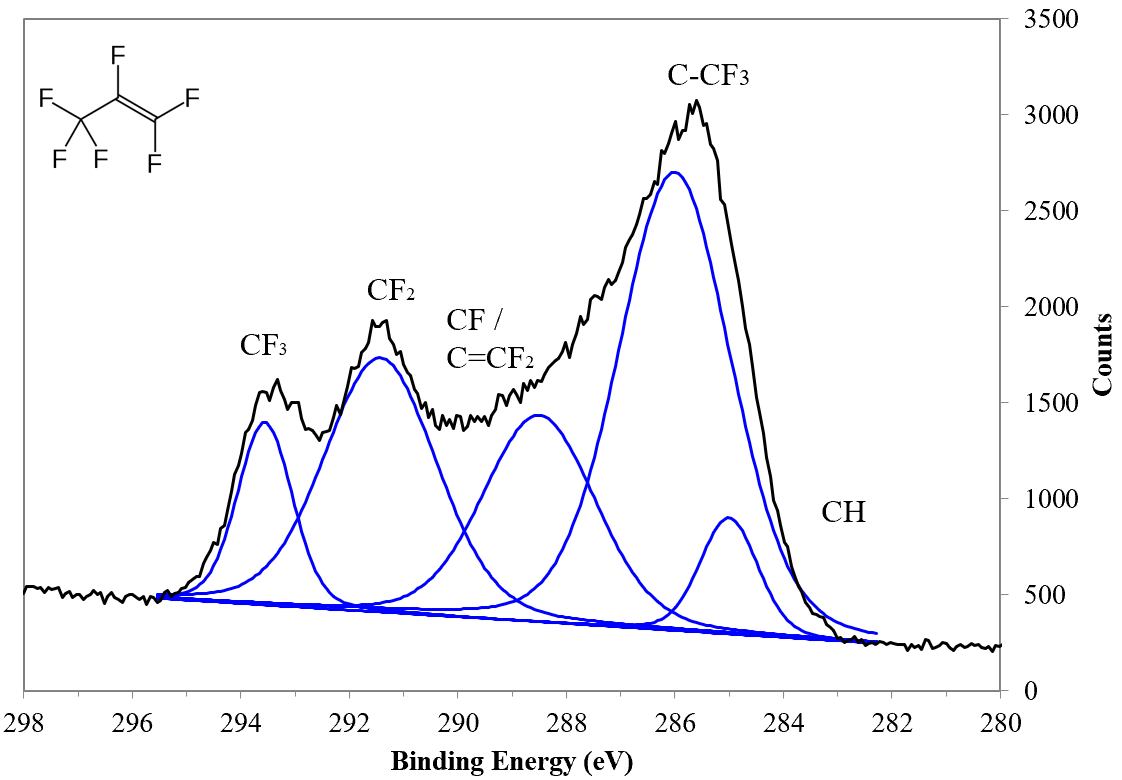

Figure 4.7 C1s spectrum of HFP (downstream) with monomer inset.

4.2.2 *Calculation of Additional Chemical Parameter*

The most basic analysis of ESCA data is to find the ratio of key elements in the survey spectra. Table 4.2 shows the average calculated F:C ratios. However, because fluorine can come in different amounts from different chemical groups, a parameter to summarize the distribution of the C1s peak envelope should be developed. This parameter is called the degree of fluorination and is calculated according to a method described by Wang et al.. (47) First, weight factors are set for the CH, CF, CF_2, and CF_3 groups based on the ratio of F to C atoms in the monomer. Then, each CF group percentage from the C1s envelope fit is multiplied by its corresponding factor. The sum of the products is the degree of fluorination, and scales logically from 0 to 3, with the number corresponding to CF_x. The calculation is straightforward for every material

except FEP and HFP, whose factors are included in Table 4.3 and Table 4.4 below. For FEP, the x in CF-CF_x was chosen to be 1.75 because x can realistically be 2 or 3.

Table 4.2 Elemental content of materials from ESCA survey scans.

Polymer	% C	% F
FEP	36.6 ± 4.9	61.9 ± 6.5
PTFE	32.0 ± 1.9	68.0 ± 1.9
PVDF	48.7 ± 1.4	51.3 ± 1.4
PVDF-HFP	47.9 ± 0.2	52.1 ± 0.2
HFP (upstream)	42.1 ± 0.3	57.9 ± 0.3
HFP (downstream)	46.1 ± 0.3	48.4 ± 0.4

Table 4.3 Weight factors for fluorination degree calculation for FEP.

Peak ID	Weight Factor (F/C)
CH	0
C-CF	1.5
CF / CF-CF_x	1.75
CF2	2
CF3	3

Table 4.4 Weight factors for fluorination degree calculation for HFP.

Peak ID	Weight Factor (F/C)
CH	0
C-CF_3	1.5
CF / C=CF_2	1
CF2	2
CF3	3

4.3 CONCLUSION

Elemental composition was obtained for each material studied, including the distribution of fluorocarbon groups, in order to confirm the following about samples: (1) handling and storage of samples was able to keep surfaces sufficiently free of environmental/hydrocarbon contamination; (2) spectra was consistent with reports in literature and made theoretical sense given the monomers used; (3) deposited coatings were different enough from each other to support experimental goals by providing a decent range in fluorine content; (4) all deposited coatings were stable under aqueous conditions, which is key for biological testing. Additionally, F:C ratio and degree of fluorination calculated from the survey and C1s spectra (respectively) were added to the list of predictors to be used in statistical analysis.

Chapter 5. ATOMIC FORCE MICROSCOPY ANALYSIS

5.1 PURPOSE

It is known that roughness can impact blood-surface interactions. Relationships between roughness and hemolysis, (48) as well as roughness and thrombogenicity (49) have previously been reported. AFM was used to generate the RMS roughness predictor variable for PCR analysis as a method to see whether differences in the physical structure of a fluoropolymer determine its protein affinity.

5.2 RESULTS AND DISCUSSION

Figure 5.1 shows the root mean square average of height deviations from the average line, also known as RMS roughness, with a gold substrate control. We immediately see that the plasma-deposited HFPs are the smoothest materials tested, and skived PTFE is the roughest, as expected. Student t-tests comparing each material to PVDF showed that all roughnesses were significantly different from that of PVDF ($p < 0.05$). While PVDF and gold were significantly different ($p < 0.05$), PVDF-HFP and gold were not ($p > 0.05$). This is curious, as it suggests the underlying substrate may have dictated the roughness for PVDF-HFP but not PVDF. It is unclear why, because the depositions were done under the same conditions and resulted in similar thicknesses (~70 nm). The following differences were also insignificant: (1) skived PTFE and stretched skived PTFE, (2) FEP and PVDF-HFP, and (3) PVDF-HFP and HFP (downstream). This means the stretching did not affect skived PTFE roughness. Figure 5.2 shows the AFM scans, from which values in Figure 5.1 were calculated. It is immediately apparent that PVDF is semicrystalline, as is expected based on the DMF solvent and spin casting method used.

According to literature, this represents primarily β-phase crystals with the highest crystallinity available for PVDF (50.6%) and large spherulites which are clearly visible in the image. (50)

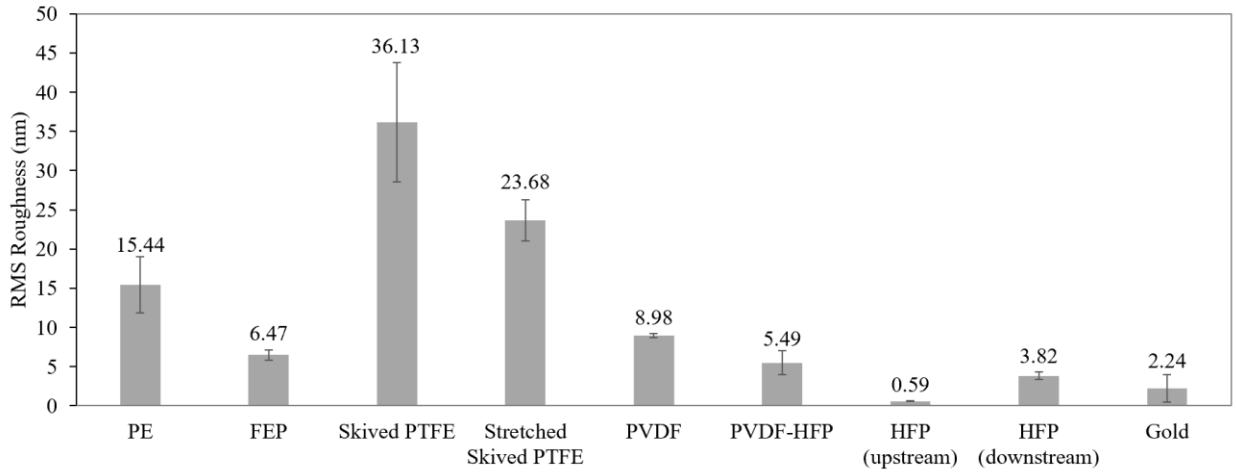

Figure 5.1 RMS roughness of all materials studied, with gold spin-coating substrate included.

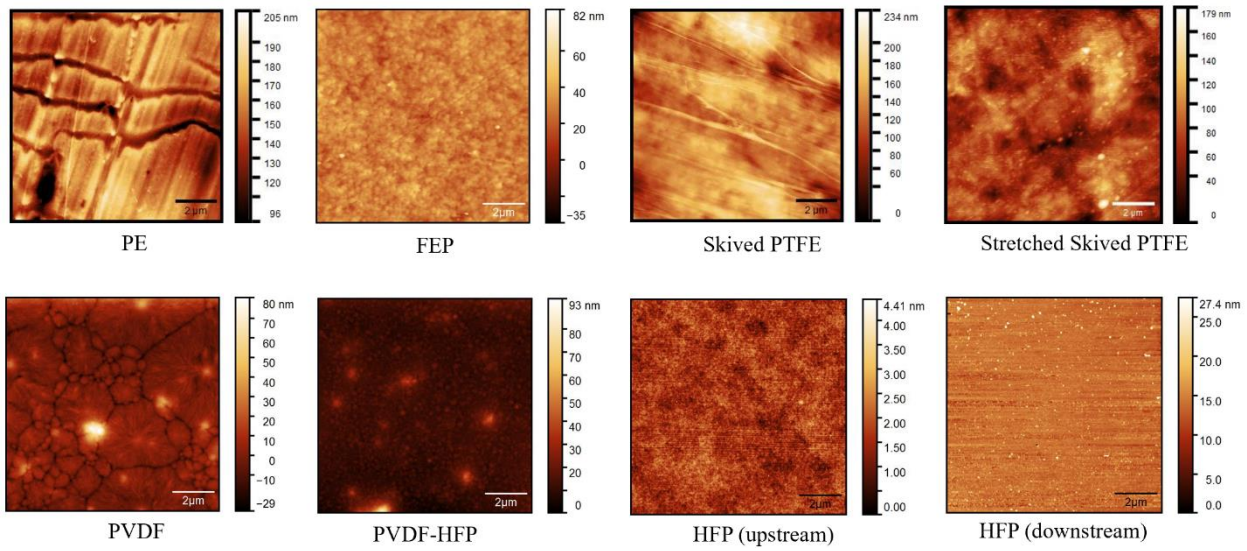

Figure 5.2 AFM tapping-mode raster scans showing material roughness. Scale bars = 2 μm.

5.3 CONCLUSION

RMS roughness was extracted from tapping-mode AFM scans of each polymer plus a gold substrate control. Plasma deposited HFP samples were found to be the smoothest, and skived PTFE the roughest, with no significant change caused in RMS roughness by stretching skived PTFE.

Chapter 6. CONTACT ANGLE ANALYSIS

6.1 PURPOSE

Surface energy is a property often studied in biomaterials due to its interfacial nature and relation with hydrophilicity. It has been shown to affect protein binding, particularly albumin. (35,51) All non-fouling surfaces have strong interaction with water, which shields the surface from protein interaction. In fact, fibrinogen adsorption has been shown to be inversely related hydrophilicity. (34) Contact angle (CA) is a highly surface-sensitive characterization technique associated with surface energy, and is also extremely easy to measure, making it the most widely used correlating factor for clinical responses to biomaterials. While CA of any liquid can be measured, water is the most relevant for biomaterials applications due to the high water content in blood and the fact that when proteins or cells approach a foreign object, they must first interact with the water molecules structured on its surface. CA is also an interesting parameter because it results from a combination of surface chemistry and roughness, both predictors included in our analysis. (8)

6.2 RESULTS AND DISCUSSION

Figure 6.1 shows the average static contact angle of water on each material, obtained using a goniometer and the sessile drop method. In general, the contact angles of the FPs measured were almost all systematically slightly lower (~7°) than published values, (52–54) possibly due to the heightened humidity of Seattle causing some water vapor to adsorb onto surfaces. (55,56) The exception was the CA for FEP, which was dramatically lower than reported values of 111° degrees. (54) This is likely due to a small level of oxygen contamination found on some FEP samples via ESCA (not previously reported because % O is not a parameter being considered).

HFP (downstream) also had a small level of oxygen, but no dramatic decrease in contact angle, which further validates the exclusion of % O from predictors. These results are unlikely to be due to hydrocarbon contamination, because the samples were rigorously cleaned and stored in nitrogen until use.

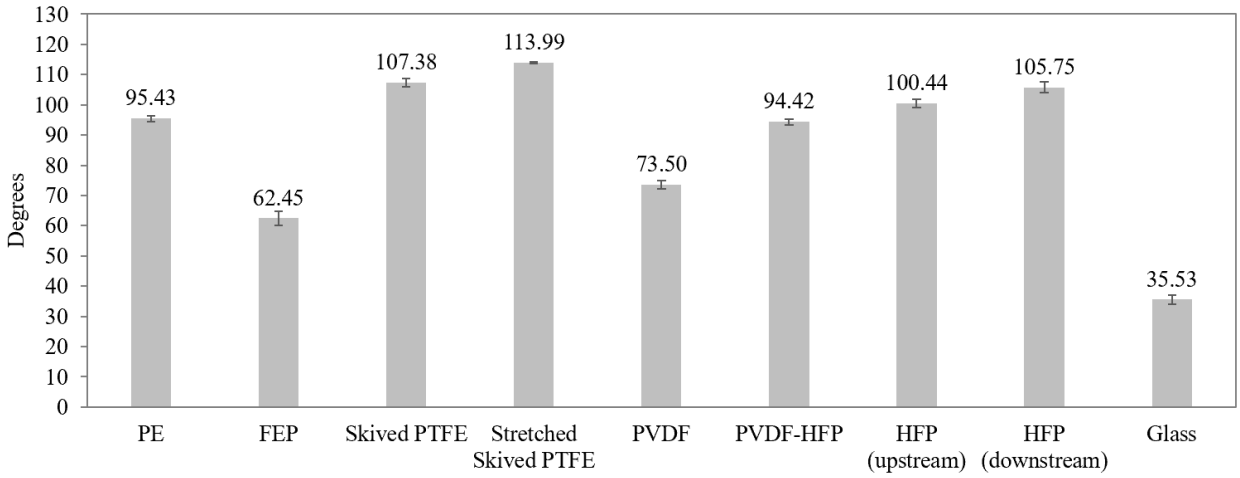

Figure 6.1 Static water contact angle of all tested materials, with glass control.

A Student t-test comparing each material to PVDF determined that all CAs were significantly different from that of PVDF ($p < 0.05$). Moreover, the following seemingly equivalent CAs were found to be significantly different: (1) skived PTFE and stretched skived PTFE, (2) HFP upstream and HFP downstream, (3) PVDF-HFP and HFP upstream. This is particularly important for the PTFE samples, as it proves that stretching did have an impact on predictors. The significant difference between the HFP samples also further validates the impact of location relative to the glow in the RFGD chamber. Without further experimentation, it remains unclear why the stretching of skived PTFE significantly impacted its contact angle, because the RMS roughness did not statistically change. It is possible that the increased chain

linearity decreased roughness in other ways that the RMS does not measure. This can be a subject for future experiments, and potentially an added predictor.

6.3 CONCLUSION

Static water contact angles were obtained for all polymers using the sessile drop method, and all materials were found to be significantly different from PVDF. The impact of stretching the skived PTFE was verified by the increase in contact angle, as was the impact of location in RFGD reactor for the HFP samples.

Chapter 7. COMPETITIVE PROTEIN ADSORPTION ANALYSIS AND PROPERTY-PERFORMANCE RELATIONSHIPS

7.1 PURPOSE

Until this point of the thesis, only predictor variables have been described and analyzed. The outcome variables in this work are parameters extracted from the competitive protein (Alb and Fbg) adsorption and retention values gathered through the radiolabeling experiments detailed in section 3.4. The radiolabeling experiments yielded values for amount protein adsorbed, amount protein retained, % protein retained, Alb:Fbg adsorbed, and Alb:Fbg retained. By comparing these data to the chemical and physical parameters already discussed, we can answer the questions in our hypotheses regarding the property-performance relationships of all the parameters measured. Note that glass is included as a standard control for radiolabeling experiments, and that PE is used as a non-fluorinated control for many figures, but neither are included in regression analysis because we are focused on teasing out property-performance relationships of fluoropolymers only.

7.2 RESULTS AND DISCUSSION

7.2.1 *Adsorption and Retention Properties*

Figure 7.1 shows the raw adsorption and retention values for albumin in parts (A) and (B), and the percent retention calculated from these values in part (C). Because PVDF is commonly used in medicine and exhibited the most interesting response, all other materials' values are tested for significance against it in two-sided unpaired Student's t-tests ($\alpha = 0.05$). One-way ANOVA with the Sidek correction was used in the case of multiple comparisons. Unstated comparisons can be

assumed to be significant. In albumin adsorption (Fig. 7.1A), all materials were significantly different from PVDF. However, no significant difference ($p > 0.05$) was found between the following comparisons: (1) skived PTFE and stretched skived PTFE, (2) PE and PVDF-HFP, (3) skived PTFE, skived stretched PTFE, PVDF-HFP, and HFP (upstream). In albumin retention (Fig. 7.1B), all materials were again significantly different from PVDF. However, no significant difference ($p > 0.05$) was found between the following comparisons: (1) skived PTFE and stretched skived PTFE, (2) HFP (upstream) and HFP (downstream), (3) HFP (downstream) and PVDF-HFP. In % albumin retained (Fig. 7.1C), all materials were found to be significantly different from PVDF except PVDF-HFP, HFP (upstream), and HFP (downstream). Additionally, no significant difference ($p > 0.05$) was found between the following comparisons: (1) skived PTFE and stretched skived PTFE, (2) skived PTFE and FEP.

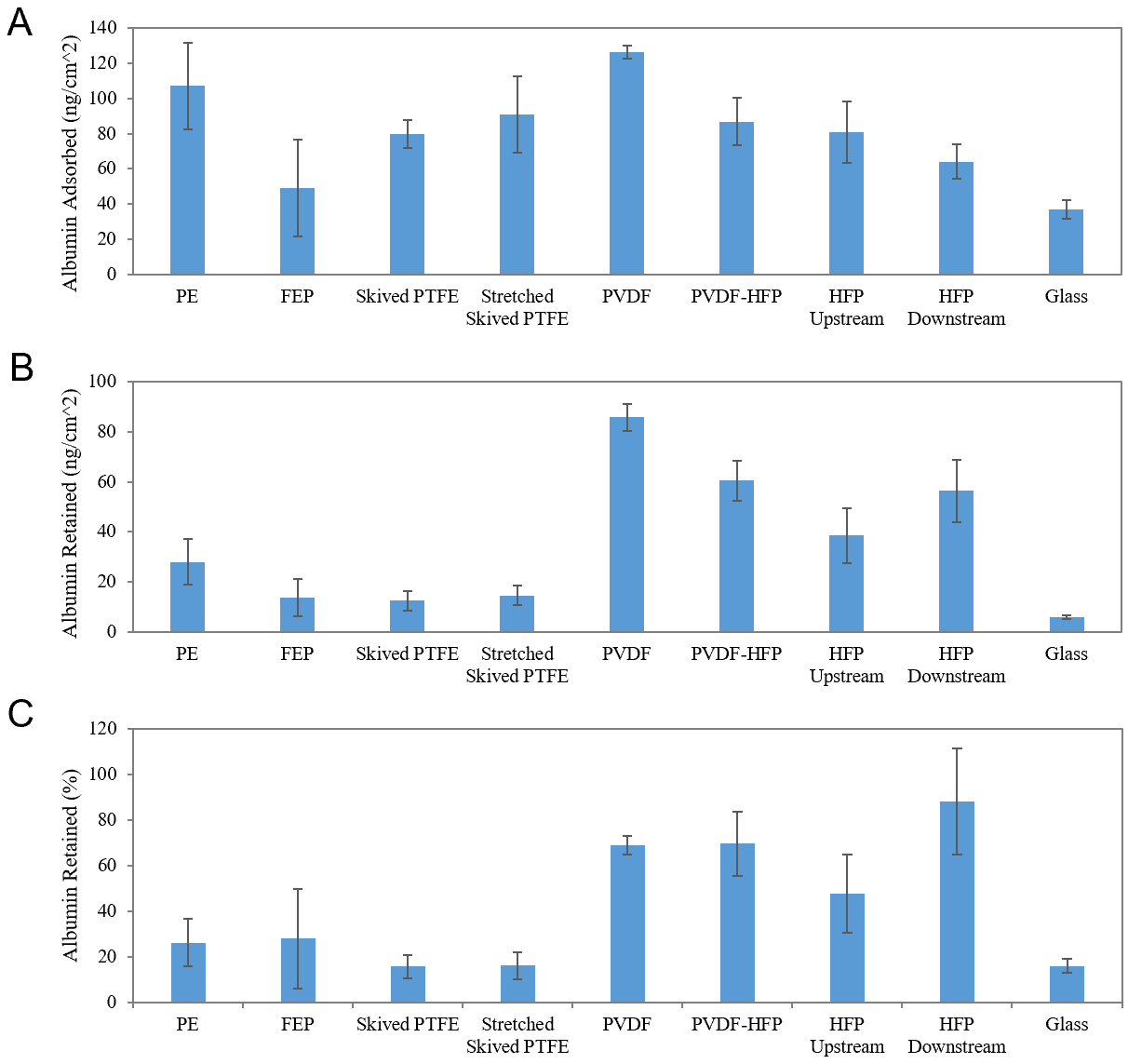

Figure 7.1 Albumin binding in binary solution. (A) Average albumin adsorbed, (B) average albumin retained, (C) percent albumin retained.

Figure 7.2 shows the raw adsorption and retention values for fibrinogen in parts (A) and (B), and the percent retention calculated from these values in part (C). PVDF is again used for testing other materials' values for significance against it in two-sided unpaired Student's t-tests ($\alpha = 0.05$). Unstated comparisons can be assumed to be significant. In fibrinogen adsorption (Fig. 7.2A), only PE and glass were significantly different from PVDF. The following combinations

also had no significant difference ($p > 0.05$): (1) skived PTFE and stretched skived PTFE, (2) HFP (downstream) and PVDF, (3) HFP (upstream) and HFP (downstream). However, a significant difference ($p < 0.05$) was found between skived PTFE and FEP. In fibrinogen retention (Fig. 7.2B), all materials were significantly different from PVDF except skived PTFE and PVDF-HFP. However, a significant difference ($p < 0.05$) was found between the following comparisons: (1) skived PTFE and stretched skived PTFE, (2) skived PTFE and PE. No significant difference ($p > 0.05$) was found between the following comparisons: (1) skived PTFE and PVDF-HFP, (2) HFP (upstream) and HFP (downstream). In % fibrinogen retained (Fig. 7.2C), no materials were found to be significantly different from PVDF except FEP, HFP (upstream), and HFP (downstream). However, a significant difference ($p < 0.05$) was found between the following comparisons: (1) skived PTFE and stretched skived PTFE, (2) HFP (upstream), and (3) HFP (downstream) were not statistically different ($p > 0.5$).

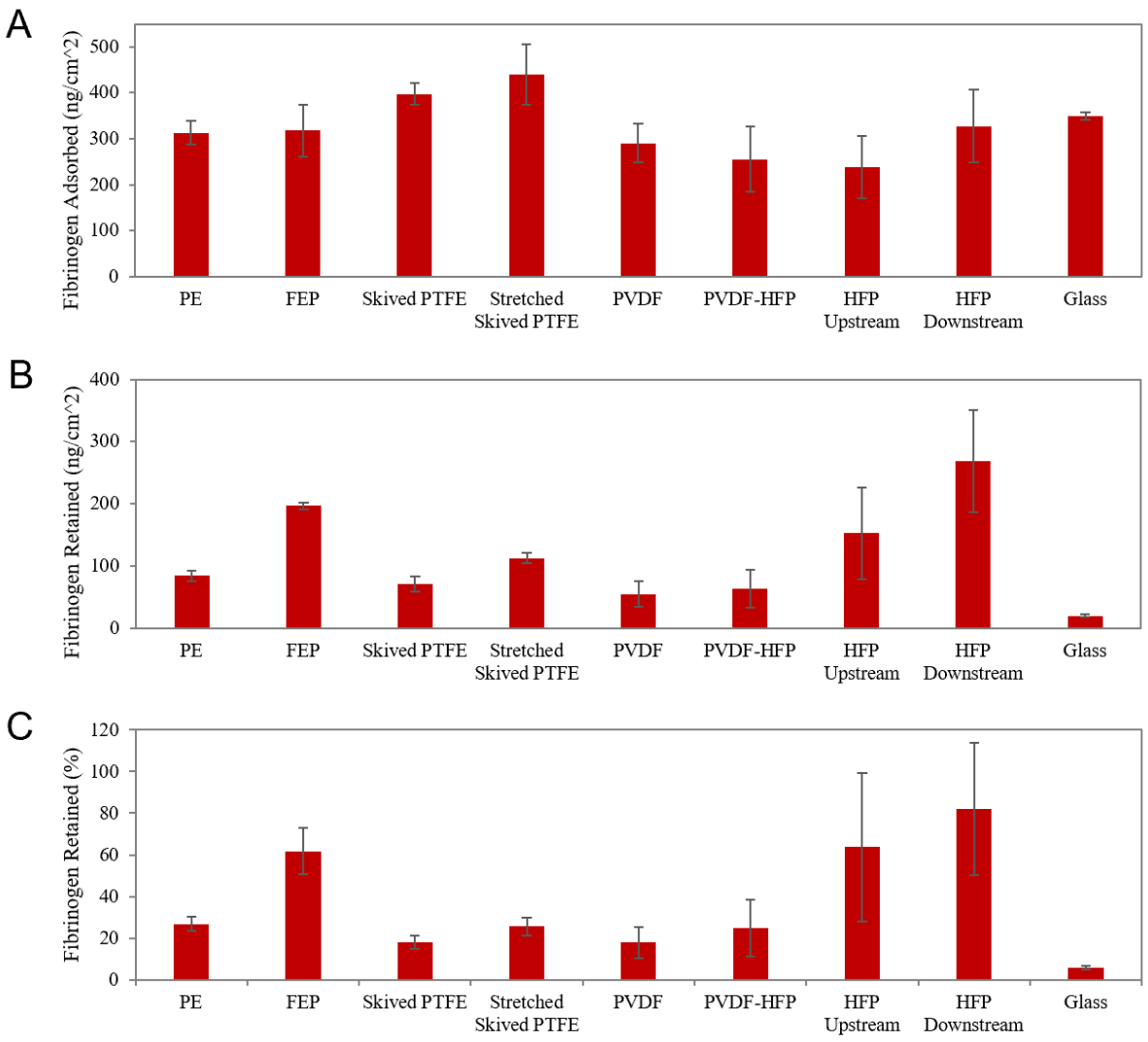

Figure 7.2 Fibrinogen binding in binary solution. (A) Average fibrinogen adsorbed, (B) average fibrinogen retained, (C) percent fibrinogen retained.

Figure 7.3 shows the ratios of albumin to fibrinogen (A) adsorption, and (B) retention. PVDF is again used for testing other materials' values for significance against it in two-sided unpaired Student's t-tests ($\alpha = 0.05$). Unstated comparisons can be assumed to be significant. In Alb:Fbg adsorption (Fig. 7.3A), all materials were significantly different from PVDF except PE, PVDF-HFP, HFP (upstream). The following combinations also had no significant difference ($p > 0.05$): (1) skived PTFE and stretched skived PTFE, (2) FEP and skived PTFE, (3) FEP and

stretched skived PTFE, (4) HFP (upstream) and HFP (downstream). In Alb:Fbg retention (Fig. 7.3B), all materials were significantly different from PVDF except PVDF-HFP. FEP and skived PTFE were significantly different ($p < 0.05$), but no significant difference ($p > 0.05$) was found between the following comparisons: (1) skived PTFE and stretched skived PTFE, (2) PE and skived PTFE, (3) FEP and skived PTFE, (4) FEP vs stretched skived PTFE, (5) HFP (upstream) and HFP (downstream).

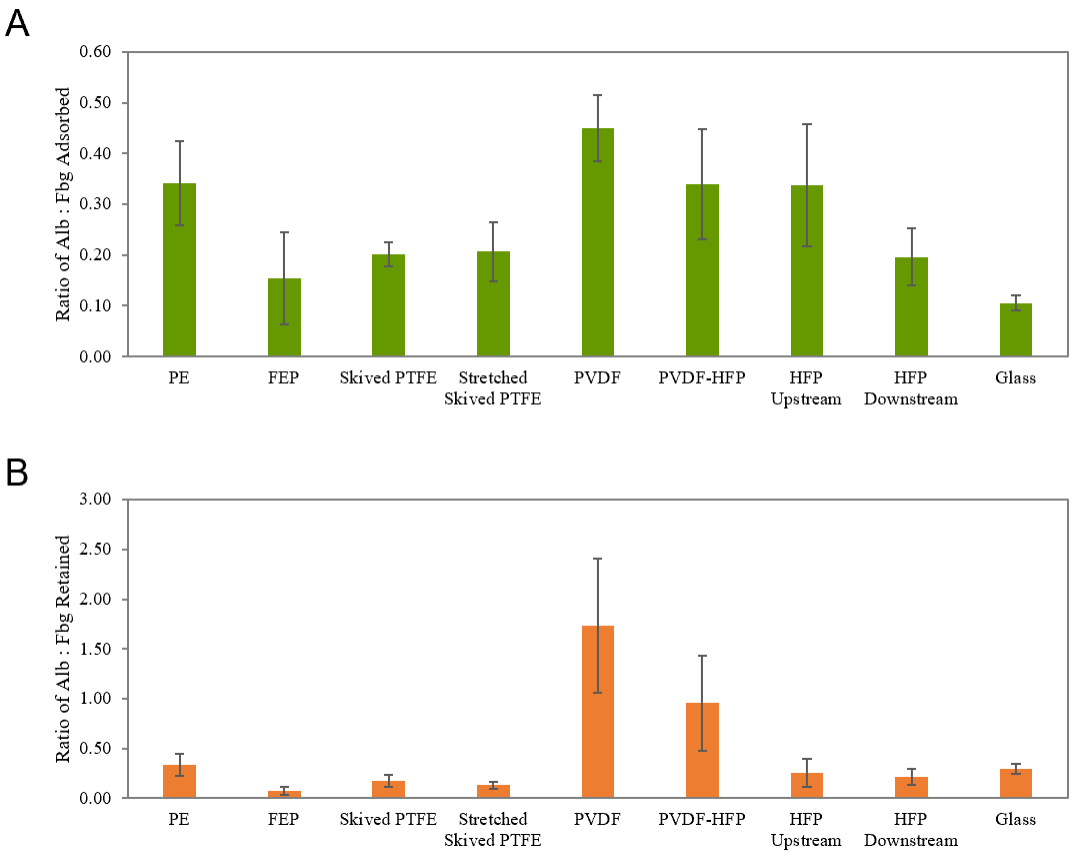

Figure 7.3 Binding ratios in binary solution. (A) Albumin to fibrinogen adsorbed, (B) Albumin to fibrinogen retained.

It is apparent in Figure 7.3A that every material tested adsorbs more fibrinogen than albumin, which makes sense given the Vroman effect. However, there are clear differences in the

adsorption ratio, hinting at initial differences in protein affinities. PVDF, PVDF-HFP, HFP (upstream), and PE have the highest Alb:Fbg adsorption ratio (statistically the same). Considering just the values without standard deviation, however, PVDF maximizes albumin adsorption. Moreover, Figure 7.3B shows that PVDF and PVDF-HFP retain the most albumin, making them initial frontrunners for material selection in the albumin tight-binding surface passivation strategy. This echoes their preferred use in the medical device industry. (11) But what about these promising candidates makes them so, and is it a property that can be maximized? To answer this question, a more sophisticated method of statistical analysis is needed.

7.2.2 *Comparison of Chemical and Physical Properties with Protein Behavior through Principal Component Analysis*

Let us first review our initial hypotheses. The first hypothesis for why different FPs prefer different proteins was that the chemical composition of the FP determines its protein affinity. As detailed earlier, there are multiple ways to define chemical composition: elemental surface composition (%C, %F) and chemical group content (%CH, %CF, %CF_2, %CF_3). However, these predictor variables are not necessarily independent of each other, requiring a more holistic picture that considers total distribution of chemical groups. We have found this in the degree of fluorination, which concisely represents the distribution of bonds in the C1s envelope. Given the observed relative superiority in albumin interaction of PVDF and PVDF-HFP, perhaps %CH and %CF_2 are the most important, but it is difficult to tell with so many parameters.

A useful tool in elegantly summarizing and assessing the potential multicollinearity in multivariate data is displaying the Pearson correlation coefficient (r) for various combinations of predictors and outcomes in a heat map. This is shown in Figure 7.4, in which it is clear that there

are many associations between the chemical and physical parameters (predictors) tested and the protein responses measured (outcomes). This makes it difficult to confidently tease out any specific relationships at face-value and precludes multiple linear regression on the raw data, since many of the predictors are correlated (shown in Figure 7.5). Thus, it behooves us to perform a more sophisticated statistical analysis to narrow the data down to a subset of necessary predictors which can be used going forward for comparison with protein response without the meddling of multicollinearity.

	Albumin Adsorbed	Fibrinogen Adsorbed	Albumin Retained	Fibrinogen Retained	Alb:Fbg Adsorbed	Alb:Fbg Retained	% Albumin Retained	% Fibrinogen Retained
CA	0.0224	0.439	-0.243	0.00627	-0.194	-0.399	-0.117	-0.0577
C	0.35	-0.784	0.942	0.0264	0.7	0.706	0.942	0.175
F	-0.187	0.706	-0.887	-0.244	-0.525	-0.562	-0.989	-0.353
CH	0.654	-0.521	0.795	-0.575	0.789	0.938	0.519	-0.481
CF	-0.367	-0.43	0.16	0.726	-0.0383	-0.326	0.497	0.851
CF2	-0.00231	0.797	-0.685	-0.428	-0.444	-0.266	-0.87	-0.613
CF3	-0.406	-0.589	-0.0301	0.544	0.0212	-0.353	0.206	0.757
F:C Ratio	-0.242	0.796	-0.903	-0.157	-0.62	-0.613	-0.963	-0.305
Fluorination Degree	-0.605	0.563	-0.912	0.388	-0.773	-0.922	-0.725	0.303
Roughness	0.122	0.823	-0.546	-0.442	-0.353	-0.233	-0.704	-0.621

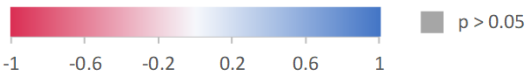

Figure 7.4 Heat map of Pearson correlation coefficient between predictors and outcomes. All non-gray values represent significant correlations.

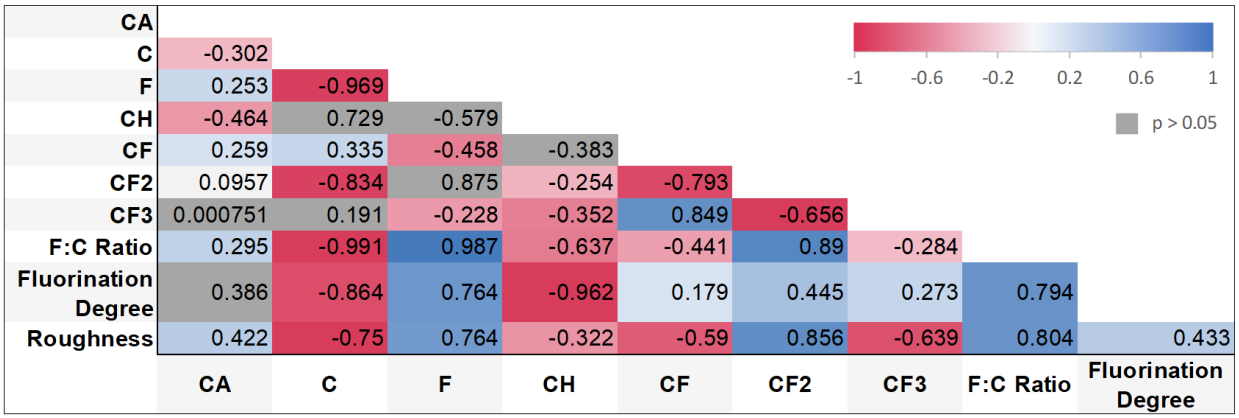

	CA	C	F	CH	CF	CF2	CF3	F:C Ratio	Fluorination Degree
CA									
C	-0.302								
F	0.253	-0.969							
CH	-0.464	0.729	-0.579						
CF	0.259	0.335	-0.458	-0.383					
CF2	0.0957	-0.834	0.875	-0.254	-0.793				
CF3	0.000751	0.191	-0.228	-0.352	0.849	-0.656			
F:C Ratio	0.295	-0.991	0.987	-0.637	-0.441	0.89	-0.284		
Fluorination Degree	0.386	-0.864	0.764	-0.962	0.179	0.445	0.273	0.794	
Roughness	0.422	-0.75	0.764	-0.322	-0.59	0.856	-0.639	0.804	0.433

Figure 7.5 Heat map of Pearson correlation coefficient amongst all predictors. All non-gray values represent significant correlations.

An appropriate approach for this task is to use principal component regression (PCR) to narrow down the most important predictors and make regression more feasible and meaningful. In addition to aiding dimensionality reduction, PCR is good for avoidance of multicollinearity between predictors and overfitting mitigation. PCR consists of principal component analysis (PCA) and linear regression. PCA is an orthogonal transformation that begins by scaling each input variable to unit variance (i.e. sample variance is one), then mapping observations of the input variables in multidimensional space. Next, ranked vectors are created in this space called principal components (PCs), which maximize the explained amount of observed variability in the predictor variables, independent of the response variables. Essentially, PCs are new, linearly uncorrelated variables that are linear combinations of the original predictor variables. The PCs are orthogonal to each other, and thus not vulnerable to multicollinearity. Each PC has a score and a loading, which come in matrices and are tied in sign (+/-). A score is an orthogonal projection on a PC line, while a loading corresponds to an original predictor and ranks how much that predictor influences the spread of the PC. (57) Thus, the first PC (PC1) explains the most variability in the dataset, following by PC2, PC3, etc.

Figure 7.6A displays the first layer of PCA results, the scree plot, which shows all the PCs identified by the algorithm. Given that over 99% of the variability in the data can be accounted for by the first four PCs, PC5 and PC6 become irrelevant to further analysis. Figure 7.6B shows the score distribution between PC1 and PC2, which together account for a vast majority of the predictor variance (87.4%) In comparing these scores, we see that similar materials are clustered together, which serves as a rudimentary internal check that the PCA model is logical and likely robust. It is interesting that the grouping seems to be based on manufacturing method. This is discussed below.

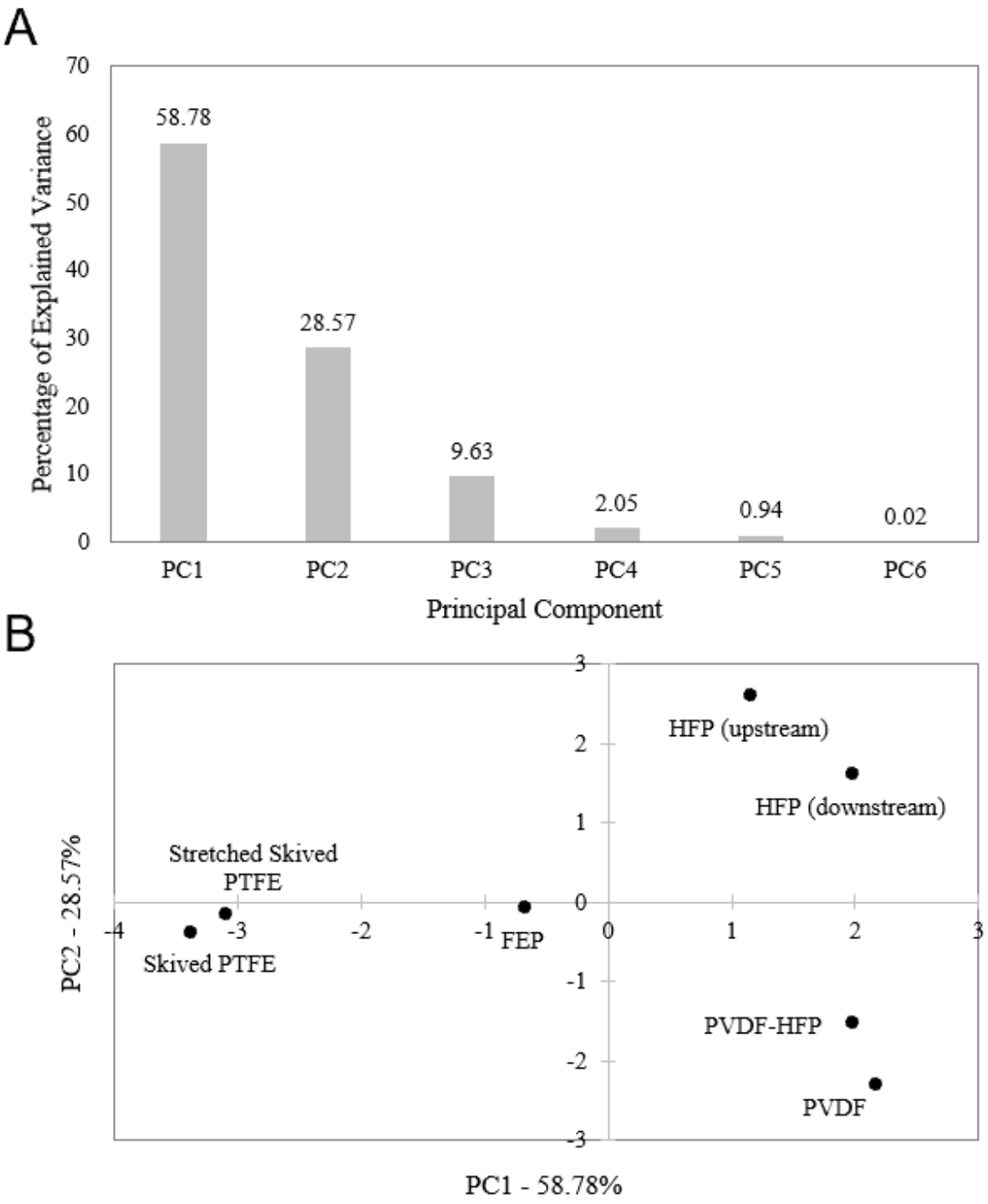

Figure 7.6 Principal Components from PCA. (A) Scree plot of all PCs, (B) Score distribution between PC1 and PC2.

Next, the protein response variables were regressed on the scores of each PC, and the adjusted coefficients of determination (R^2) recorded in Table 7.1. A negative adjusted R^2 denotes

that the tested model contained variables that did not predict the response, and p-value is only reported for fits that were significant. PC1 was able to explain 67% of the variation in the amount of fibrinogen adsorbed, and 83% of the variation in the percent of albumin retained. Meanwhile, PC2 was able to explain 40% of the variation in the amount of the ratio of Alb:Fbg retained, and 56% of the variation in the percent of fibrinogen retained. Most of the p-values are insignificant due to low sample size.

Table 7.1 Adjusted R^2 from simple linear regression (** $p < 0.05$, * $p < 0.1$).

PC	Albumin Adsorbed	Fibrinogen Adsorbed	Alb:Fbg Adsorbed	Alb:Fbg Retained	% Alb Retained	% Fbg Retained
PC1	-0.1512	** ***0.6672***	0.2603	0.2043	** ***0.8310***	-0.0488
PC2	0.1935	-0.1867	-0.0337	* 0.4018	-0.2000	** ***0.5576***
PC3	-0.0522	-0.1181	-0.1727	-0.1875	-0.0956	-0.1280
PC4	-0.0598	-0.0591	0.0860	-0.1717	-0.1382	-0.0289
PC5	-0.1372	-0.1514	-0.0989	-0.1451	-0.1985	-0.1619
PC6	0.2069	-0.1519	-0.0409	-0.1018	-0.1988	-0.1900

Figure 7.7 shows the scores of PC1 relevant from principal component regression. It is apparent that a more negative score corresponds to a higher amount of fibrinogen adsorbed, while a more positive score corresponds to higher % albumin retention. The PC1 loadings are shown in Table 7.2, and correspond to the PC1 scores in terms of sign. Therefore, F:C ratio corresponds most with higher amount Fbg adsorbed, followed by %F and %CF2, then roughness. Additionally, % C corresponds with higher % albumin retention, followed by % CH. By using this selection criteria and extracting Pearson correlation coefficients from Figure 7.4, we can say that for fibrinogen adsorption there is a very strong positive association with F:C Ratio ($r = 0.796$), a strong positive association with %F ($r = 0.706$), and very strong positive associations with $\%CF_2$ ($r = 0.797$) and roughness ($r = 0.823$). For % albumin retention, there is a very strong

positive association with %C (r = 0.942), and a moderate positive association with %CH (r = 0.519).

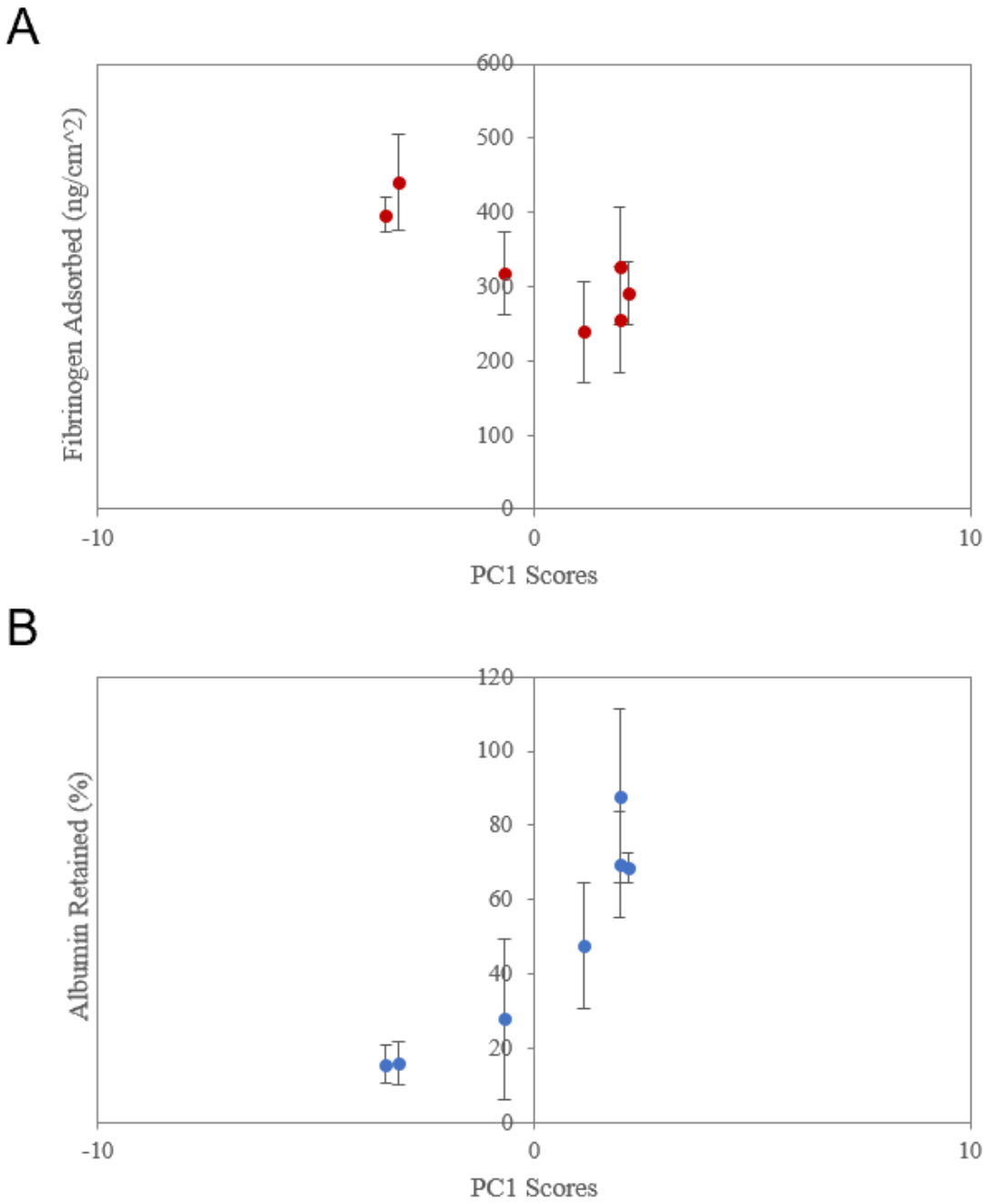

Figure 7.7 Scores of principal component 1 relevant from principal component regression.

Table 7.2 Loadings of principal component 1.

Parameter	Loading
CH	-0.4462
CF_2	-0.2394
Roughness	-0.1652
C	-0.0969
F	0.0228
F:C Ratio	0.0300
Contact Angle	0.2347
Fluorination Degree	0.3739
CF_3	0.4978
CF	0.5126

Figure 7.8 shows the scores of PC2 relevant from principal component regression. It is apparent that a more negative score corresponds to a higher ratio of Alb:Fbg retained, while a more positive score corresponds to higher % fibrinogen retention. The PC2 loadings are shown in Table 7.3, and correspond to the PC2 scores in terms of sign. Therefore, %CH corresponds with higher ratio of Alb:Fbg retained, while %CF corresponds with higher % fibrinogen retained, followed by $\%CF_3$, then fluorination degree. By using this selection criteria and extracting Pearson correlation coefficients from Figure 7.4, we can say that for the ratio of Alb:Fbg retained, there is a very strong positive association with %CH ($r = 0.938$). Additionally, for % fibrinogen retention, there is a very strong positive association with %CF ($r = 0.851$), a moderate positive association with $\%CF_3$ ($r = 0.757$), and a weak positive association with fluorination degree ($r = 0.303$).

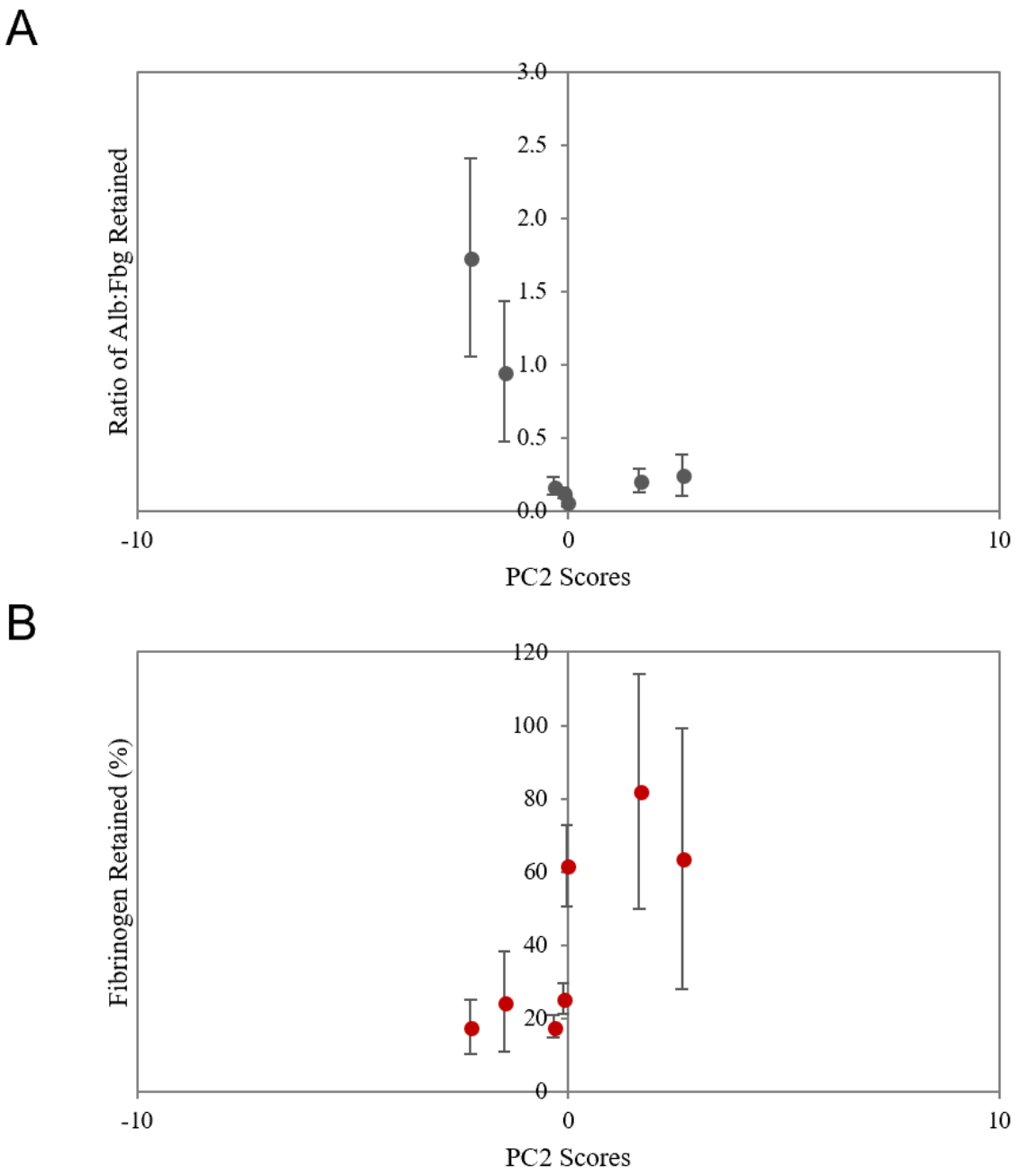

Figure 7.8 Scores of principal component 2 relevant from principal component regression.

Table 7.3 Loadings of principal component 2.

Parameter	Loading
Contact Angle	-0.8420
Roughness	-0.3176
C	-0.1401
CF	-0.1269
CH	-0.0263
CF_2	0.0919
F:C Ratio	0.1091
Fluorination Degree	0.1537
F	0.1677
CF_3	0.2859

In revisiting our first hypothesis, which was that the chemical composition of a FP determines its protein affinity, with CH and CF_2 content playing important roles, we find that the PCR results support this hypothesis. However, other chemical parameters (F:C ratio, %CF) play important roles too and may be even better predictors of protein response. Moreover, with the current data available we are only able to find substantial relationships to the following protein responses: amount fibrinogen adsorbed, % albumin retained, ratio of Alb:Fbg retained, and % fibrinogen retained.

Our second hypothesis is that differences in the physical structure of a FP determine its protein affinity, namely through roughness and manufacturing method. Unfortunately, manufacturing methods could not statistically be compared without explicit knowledge of the PE and FEP film creation, but it is interesting to note how the data in Figure 7.6B are clustered based on manufacturing method and not necessarily chemical similarity, suggesting that the method of manufacturing may influence protein behavior on a surface. Additionally, the materials with the greatest preference for retaining albumin (PVDF and PVDF-HFP, shown in Figure 7.3B) are both spin-cast. A true test of the effect of manufacturing would be to deposit the

same polymer solution in multiple ways (e.g. spin coating, plasma deposition, etc), but the solvent resistance of FPs makes this a tricky problem outside the scope of this thesis.

Roughness was also found to impact protein adsorption to a more limited extent than other parameters, which is supported in literature. (49) Recall from the PCA results that PC1 identified roughness as having a very strong positive association with fibrinogen adsorption ($r = 0.823$), and that Figure 7.4 also showed roughness to have strong negative correlations with the percent retention of albumin ($r= -0.709$) and fibrinogen ($r= -0.621$). PCR did not identify roughness as a useful predictor for any protein response other than fibrinogen adsorption. These points suggest that while a rougher surface may initially adsorb more fibrinogen, it does not aid in retention. This hypothesis can be explored in the future using techniques such as surface plasmon resonance or quartz crystal microbalance with dissipation monitoring.

To test our surface energy hypothesis, the plastic deformation of skived PTFE along its skiving direction was utilized to increase chain alignment, thereby impacting its surface energy. A t-test to determine if the differences in protein response are significant between skived PTFE and stretched skived PTFE only yielded significant differences in the % fibrinogen retained, with stretched skived PTFE retaining more fibrinogen. Given that the RMS roughnesses of these two materials were not statistically different ($p > 0.05$), while their static water contact angles were ($p < 0.05$), we can assume that the stretching successfully changed the surface energy, but we cannot be certain as to how. Thus, we conclude that under the conditions tested, surface energy likely does determine protein binding affinity (specifically, of fibrinogen). To gain more mechanistic insight into why, larger sample size and additional techniques - such as profilometry and more complicated and costly surface orientation analysis techniques like Near Edge X-Ray Absorption Fine Structure (NEXAFS) - but this is beyond the scope of this thesis.

While we have answered our hypotheses, it would be desirable to also have predictive information on the amount of albumin adsorbed, and higher coefficients of determination in the PCR. It should be noted that PCR identified parameters that do not necessarily have the highest individual correlation with the corresponding outcome, because they account for the most variability in the entire data set. This is usually caused by nonlinearity and compound effects. The limitations of this analysis are that it deals only in linear models, and that the data has a low sample size. These points do not discredit the PCR model, however, especially since it accurately grouped the materials in Figure 7.6B. They merely suggest that with repetition of experiments, we can increase our power to determine whether certain relationships are nonlinear, and adjust the statistical analysis accordingly. Increasing sample size would also likely improve the significance of the regression fits, and thus our predictive power. Nevertheless, these methods of analysis and preliminary results have already begun to serve as useful tools for the rational design of tight-binding fluoropolymers.

7.2.3 *Conclusions*

The adsorption of albumin and fibrinogen under competitive binding conditions was measured via radiolabeling, and the results were indirectly regressed on the predictor variables (from ESCA, AFM, contact angle measurement) using PCR to account for multicollinearity. All the materials tested adsorbed more fibrinogen than albumin due to the Vroman effect, but some retained more albumin than fibrinogen (PVDF and PVDF-HFP). The results of hypothesis testing suggest that various chemical composition parameters, roughness, and orientation of CF_2 groups in FPs all help determine protein affinity.

Based on the results obtained, the following preliminary property-performance guidelines are recommended. For preferential albumin retention, it is desirable to have high carbon content, coming from CH. For preferential fibrinogen adsorption, it is desirable to have higher fluorine content, particularly from CF_2, and higher roughness. For preferential fibrinogen retention, it is desirable to have higher CF content. Note that these recommendations apply to FPs only, and maximizing only one property will likely not result in the desired outcome, because PCR results indicate the influence of compound effects. For example, while % C and %CH are associated with stronger albumin binding, PE, which is pure hydrocarbon, does not exhibit the highest albumin retention. The most promising materials to move forward with regarding the achievement of albumin tight-binding appear to be PVDF, PVDF-HFP, and HFP deposited upstream of the glow, with PVDF being the initial frontrunner. This is promising for scaling up of production because PVDF has a good performance to cost ratio. (58)

Finally, it should be noted that it is likely some of these property-performance relationships are not linear. Recommendations are derived from linear models, and while initial indications suggest the model is robust, more data replicates should be obtained to validate these results. Should non-linear relationships be found, the more mechanistic experiments required to assign physical meaning to such more complex models would be beyond the scope of this project.

Chapter 8. SUMMARY

8.1 CONCLUSIONS

For decades, the following phenomena have been known: (1) protein adsorption on biomaterials directs platelet and other cellular responses, (2) fluoropolymer coatings on medical devices can decrease their thrombogenicity, and (3) different fluoropolymers exhibit different affinities for blood proteins. While much research has been conducted to measure protein binding and platelet adhesion on these and other surfaces, there is still no definite explanation for the observed phenomena, and thus insufficient understanding of how to rationally design cardiovascular device coatings that are biocompatible enough to not need pharmaceutical anticoagulation. The work herein represents a refreshed approach to this problem.

With the goal of teasing out property-performance relationships for fluoropolymers and surface-protein interactions, the following predictor variables were collected: elemental composition and chemical group content from ESCA spectra, static water contact angle with a goniometer, and RMS roughness from AFM. Studying a relatively high number of FPs allowed us to have a range of predictor values necessary for observing trends with the outcome variables, which refer to various protein response parameters. These parameters are adsorbed and retained albumin and fibrinogen, calculated % retention of each protein, and ratios of Alb:Fbg adsorbed and retained. Principal component regression was utilized to decrease dimensionality, and identify the most influential properties while taking into account predictor multicollinearity.

We have shown that the preferential protein adsorption and retention of FPs is related to several chemical and physical parameters, but that none of these parameters work alone. The adsorption of albumin and fibrinogen under competitive binding conditions was measured via

radiolabeling, and the results were indirectly regressed on the predictor variables (from ESCA, AFM, contact angle measurement) using PCR to account for multicollinearity. All the materials tested adsorbed more fibrinogen than albumin due to the Vroman effect, but some retained more albumin than fibrinogen (PVDF and PVDF-HFP). The results of hypothesis testing suggest that various chemical composition parameters, roughness, and surface energy in FPs all help determine protein affinity. While this is a somewhat obvious conclusion, the experimental design enables us to go a step further in analysis, which has not yet been reported.

Based on the PCR, the following property-performance guidelines are recommended. For preferential albumin retention, it is desirable to have high carbon content, coming from CH. For preferential fibrinogen adsorption, it is desirable to have higher fluorine content, particularly from CF_2, and higher roughness. For preferential fibrinogen retention, it is desirable to have higher CF content. Note that these recommendations apply to FPs only, and maximizing only one property will likely not result in the desired outcome, because PCR results indicate the influence of compound effects. The most promising materials to move forward with regarding the achievement of albumin tight-binding appear to be PVDF, PVDF-HFP, and HFP deposited upstream of the glow, with PVDF being the initial frontrunner. This is promising for scaling up of production because PVDF has a good performance to cost ratio.

The PCR model robustly demonstrates that compound and possibly also non-linear relationships exist, and that in order to gain better predictive power a higher sample size must be obtained. Nevertheless, these methods of analysis and preliminary results already begin to serve as useful tools for the rational design of tight-binding fluoropolymers.

8.2 Future Work

This thesis comprises the first part of a multi-pronged project aimed at designing a fluoropolymer coating for blood-contacting devices that minimizes or eliminates the need for anticoagulation. Part two will be an extension of experiments to include platelet adhesion and spreading. Given that the ultimate goal is to develop a FP that minimizes thrombosis, which is closely related to platelet activation, the next logical step in this project is to expose human platelets to the same FPs and quantify their morphologies. Progress has been made toward this, but the results are beyond the scope of this thesis and require further optimization of platelet source to ensure reproducibility. Nevertheless, the following aspects essential to the success of this future work have been determined and are detailed in Appendices B and C, respectively:

1. selection and titration of fluorescent probe to identify the presence or absence of platelets on surfaces that appear bare under SEM (this can occur with fully spread platelets)
2. protocol development for the separation of blood to obtain platelet rich plasma, as well as subsequent platelet deposition, fixing, and imaging.

With the framework for this entire project in place, the platelet response data can be added into the analysis performed in this thesis. Doing so will allow us to determine why platelets spread more on particular fluoropolymer surfaces than others. Under the hypothesis that fully spread platelets passivate their substrates to further blood reactions, this information can then be translated into suggestions for the type of composition and possibly manufacturing method a FP coating should have to maximize platelet spreading. Foreseeable challenges include:

1. obtaining a better understanding of how FP surfaces dictate protein-platelet interactions on a mechanistic level, which can be accomplished via a combination of QCMD and probing fibrinogen binding site availability with antibodies;
2. quantifying thromboembolization of surfaces with full platelet spreading, for which an appropriate thrombin generation assay must be selected and flow conditions decided;
3. testing the efficacy of the "optimal" suggested FP over time in-vivo (to show potential for self-replenishment of fully spread platelet layer), which can be done in an arteriovenous shunt model in sheep.

While the tasks and obstacles standing before the implementation of an optimized FP coating in the AKTIV portable hemodialyzer are many, the work described herein represents a major stride toward their realization, having developed foundational procedures, data, design recommendations, and experimental infrastructure, as well as broken down the problem into workable parts to launch additional projects. With the mobilization of a team to undertake the remaining work, the author remains hopeful that this much-needed, refreshed approach to solving the decades-old biocompatibility problem will help improve the lives of dialysis and other medical device patients that the resulting product will reach.

BIBLIOGRAPHY

1. Chemours. History of Teflon [Internet]. [cited 2018 Aug 2]. Available from: https://www.chemours.com/Teflon/en_US/products/history.html

2. Drobny JG. Fluoropolymers in automotive applications. Polym Adv Technol. 2006;18:117–21.

3. Leveen HH, Barberio JR. Tissue Reaction to Plastics Used in Surgery with Special Reference to Teflon. Ann Surg. 1949 Jan;129(1):74–84.

4. Soyer T, Lempinen M, Cooper P, Norton L, Eiseman B. A new venous prosthesis. Surgery. 1972 Dec;72(6):864–72.

5. Matsumoto H, Hasegawa T, Fuse K, Yamamoto M, Saigusa M. A new vascular prosthesis for a small caliber artery. Surgery. 1973 Oct;74(4):519–23.

6. Fluoropolymers Market Research Report – Global Forecast to 2023. 2018.

7. Smart BE. Characteristics of C-F Systems. In: Organofluorine Chemistry. Boston, MA: Springer US; 1994. p. 57–88.

8. Ratner BD. Biomaterials Science : An Introduction to Materials in Medicine. 3rd ed. Academic Press; 2013.

9. Drobny J. Fluoroplastics. 16th ed. Rapra Technology Ltd; 2006.

10. Howard AJ, Rye RR, Houston JE. Nanomechanical basis for imaging soft materials with tapping mode atomic force microscopy. J Appl Phys. 1996;79(1885):2613.

11. Szott LM, Irvin CA, Trollsas M, Hossainy S, Ratner BD. Blood compatibility assessment of polymers used in drug eluting stent coatings. Biointerphases. 2016;11(2):029806.

12. Shard AG. Plasma assisted thin film formation. Durham University; 1992.

13. Sharma AK. Reproducibility in glow discharge polymerization. J Polym Sci Part A Polym Chem. 1986 Nov 1;24(11):3077–87.

14. Sottiurai VS. Technique in direct venous valvuloplasty. J Vasc Surg. 1988 Nov 1;8(5):646–8.

15. Kannan RY, Salacinski HJ, Butler PE, Hamilton G, Seifalian AM. Current status of prosthetic bypass grafts: A review. J Biomed Mater Res Part B Appl Biomater. 2005 Jul;74B(1):570–81.

16. DeBord JR. THE HISTORICAL DEVELOPMENT OF PROSTHETICS IN HERNIA SURGERY. Surg Clin North Am. 1998 Dec;78(6):973–1006.

17. Mascarenhas R, MacDonald PB. Anterior cruciate ligament reconstruction: a look at prosthetics--past, present and possible future. Mcgill J Med. 2008 Jan;11(1):29–37.

18. Gallagher SR. Protein Blotting: Immunoblotting. In: Current Protocols Essential Laboratory Techniques. Hoboken, NJ, USA: John Wiley & Sons, Inc.; 2010. p. 8.3.1-8.3.36.

19. Winslow RM. Blood substitutes. Elsevier Academic Press; 2006. 259-323 p.

20. Yu Q, Liu K, Su L, Xia X, Xu X. Perfluorocarbon liquid: its application in vitreoretinal surgery and related ocular inflammation. Biomed Res Int. 2014 Mar 30;2014:250323.

21. Scalamone JC. Fluorine containing soft contact lens hydrogels. US5684059A, 1995.

22. Kamberi M, Pinson D, Pacetti S, Perkins LEL, Hossainy S, Mori H, et al. Evaluation of chemical stability of polymers of XIENCE everolimus-eluting coronary stents *in vivo* by pyrolysis-gas chromatography/mass spectrometry. J Biomed Mater Res Part B Appl Biomater. 2018 Jul;106(5):1721–9.

23. Mozaffarian D, Benjamin EJ, Go AS, Arnett DK, Blaha MJ, Cushman M, et al. Heart Disease and Stroke Statistics—2016 Update. Circulation. 2016 Jan 26;133(4):e38–360.

24. Sercombe L, Veerati T, Moheimani F, Wu SY, Sood AK, Hua S. Advances and Challenges of Liposome Assisted Drug Delivery. Front Pharmacol. 2015 Dec 1;6:286.

25. Achneck HE, Sileshi B, Parikh A, Milano CA, Welsby IJ, Lawson JH. Pathophysiology of

Bleeding and Clotting in the Cardiac Surgery Patient: From Vascular Endothelium to Circulatory Assist Device Surface. Circulation. 2010 Nov 16;122(20):2068–77.

26. Bhatia S. Systems for Drug Delivery : Safety, Animal, and Microbial Polysaccharides. Switzerland: Springer International Publishing; 2016. 1-9 p.

27. Ratner BD. The catastrophe revisited: Blood compatibility in the 21st Century. Biomaterials. 2007;28(34):5144–7.

28. Gupta S, Reviakine I. Platelet Activation Profiles on TiO2: Effect of Ca2+ Binding to the Surface. Biointerphases . 2012;7(28).

29. Wu Y, Simonovsky FI, Ratner BD, Horbett TA. The role of adsorbed fibrinogen in platelet adhesion to polyurethane surfaces: A comparison of surface hydrophobicity, protein adsorption, monoclonal antibody binding, and platelet adhesion. J Biomed Mater Res Part A. 2005 Sep 15;74A(4):722–38.

30. Hirsh SL, McKenzie DR, Nosworthy NJ, Denman JA, Sezerman OU, Bilek MMM. The Vroman effect: Competitive protein exchange with dynamic multilayer protein aggregates. Colloids Surfaces B Biointerfaces. 2013 Mar 1;103:395–404.

31. Bailly A-L, Laurent A, Lu H, Elalami I, Jacob P, Mundler O, et al. Fibrinogen binding and platelet retention: Relationship with the thrombogenicity of catheters. J Biomed Mater Res. 1996 Jan 1;30(1):101–8.

32. Ji J, Feng L, Barbosa MA. Stearyl poly(ethylene oxide) grafted surfaces for preferential adsorption of albumin. Biomaterials. 2001 Nov;22(22):3015–23.

33. Paulsson M, Kober M, Freij-Larsson C, Stollenwerk M, Wesslén B, Ljungh Å. Adhesion of staphylococci to chemically modified and native polymers, and the influence of preadsorbed fibronectin, vitronectin and fibrinogen. Biomaterials. 1993 Sep 1;14(11):845–53.

34. Rodrigues SN, Gonçalves IC, Martins MCL, Barbosa MA, Ratner BD. Fibrinogen adsorption, platelet adhesion and activation on mixed hydroxyl-/methyl-terminated self-

assembled monolayers. Biomaterials. 2006 Nov 1;27(31):5357–67.

35. Kiaei D, Hoffman AS, Horbett TA. Tight binding of albumin to glow discharge treated polymers. J Biomater Sci Polym Ed. 1993 Jan 1;4(3):35–44.

36. Bohnert JL, Fowler BC, Horbett TA, Hoffman AS. Plasma gas discharge deposited fluorocarbon polymers exhibit reduced elutability of adsorbed albumin and fibrinogen. J Biomater Sci Polym Ed. 1990;1(4):279–97.

37. Cass T, Ligler FS. Immobilized biomolecules in analysis : a practical approach. Oxford University Press; 1998. 216 p.

38. Paynter R., Ratner B., Horbett T., Thomas H. XPS studies on the organization of adsorbed protein films on fluoropolymers. J Colloid Interface Sci. 1984 Sep 1;101(1):233–45.

39. Hylton DM, Shalaby SW, Latour RA. Direct correlation between adsorption-induced changes in protein structure and platelet adhesion. J Biomed Mater Res Part A. 2005 Jun 1;73A(3):349–58.

40. Helmkamp RW, Contreras MA, Bale WF. I131-Labeling of Proteins by the Iodine Monochloride Method. Vol. 18, International Journal of Applied Radiation and Imtopes. Pergamon Press Ltd; 1967.

41. Horbett TA. Adsorption of proteins from plasma to a series of hydrophilic-hydrophobic copolymers. II. Compositional analysis with the prelabeled protein technique. J Biomed Mater Res. 1981 Sep 1;15(5):673–95.

42. Sastri VR. Plastics in Medical Devices: PROPERTIES, REQUIREMENTS, AND APPLICATIONS. William Andrew Publishing; 2010. 73-119 p.

43. Shi M-K, Lamontagne B, Selmani A, Martinu L. X-ray photoelectron spectroscopy study of x-ray irradiated metal/fluoropolymer interfaces. J Vac Sci Technol A. 1994;12(44):44–50.

44. Hinckley AC, Wang C, Pfattner R, Kong D, Zhou Y, Ecker B, et al. Investigation of a

Solution-Processable, Nonspecific Surface Modifier for Low Cost, High Work Function Electrodes. ACS Appl Mater Interfaces. 2016 Aug 3;8(30):19658–64.

45. Luginbühl R, Szuchmacher A, Garrison MD, Lhoest J-B, Overney RM, Ratner BD. Comprehensive surface analysis of hydrophobically functionalized SFM tips. Ultramicroscopy. 2000 Feb 1;82(1–4):171–9.

46. Garrison MD, Luginbühl R, Overney RM, Ratner BD. Glow discharge plasma deposited hexafluoropropylene films: surface chemistry and interfacial materials properties. Thin Solid Films. 1999 Sep 8;352(1–2):13–21.

47. Wang Z, Wang J, Li Z, Gong P, Liu X, Zhang L, et al. Synthesis of fluorinated graphene with tunable degree of fluorination. Carbon N Y. 2012 Dec 1;50(15):5403–10.

48. Wielogorski JW, Davy TJ, Regan RJ. The influence of surface rugosity on haemolysis occurring in tubing. Biomed Eng (NY). 1976 Mar;11(3):91–4.

49. Hecker JF, Scandrett LA. Roughness and thrombogenicity of the outer surfaces of intravascular catheters. J Biomed Mater Res. 1985 Apr;19(4):381–95.

50. Ma W, Zhang J, Chen S, Wang X. Crystalline Phase Formation of Poly(vinylidene fluoride) from Tetrahydrofuran/N,N-dimethylformamide Mixed Solutions. J Macromol Sci Part B. 2008 Apr 2;47(3):434–49.

51. Michiardi A, Aparicio C, Ratner BD, Planell JA, Gil J. The influence of surface energy on competitive protein adsorption on oxidized NiTi surfaces. Biomaterials. 2007 Feb 1;28(4):586–94.

52. du Toit FJ, Sanderson RD, Engelbrecht WJ, Wagener JB. The effect of surface fluorination on the wettability of high density polyethylene. J Fluor Chem. 1995 Sep 1;74(1):43–8.

53. Lee L-H. Characterization of Metal and Polymer Surfaces V2 : Polymer Surfaces. Elsevier Science; 1977. 324 p.

54. Li D, Neumann A. Contact angles on hydrophobic solid surfaces and their interpretation. J Colloid Interface Sci. 1992 Jan 1;148(1):190–200.

55. Weisensee PB, Neelakantan NK, Suslick KS, Jacobi AM, King WP. Impact of air and water vapor environments on the hydrophobicity of surfaces. J Colloid Interface Sci. 2015;453:177–85.

56. Wakai C, Shimoaka T, Hasegawa T. Characterization of Adsorbed Molecular Water on the Surface of a Stretched Polytetrafluoroethylene Tape Analyzed by 1 H NMR. 2016;

57. Wold S, Esbensen K, Geladi P. Principal component analysis. Chemom Intell Lab Syst. 1987 Aug 1;2(1–3):37–52.

58. Material Properties - PVDF.

APPENDIX A - FIXTURE DESIGN FOR DOUBLE-SIDED ELECTRON BEAM EVAPORATION

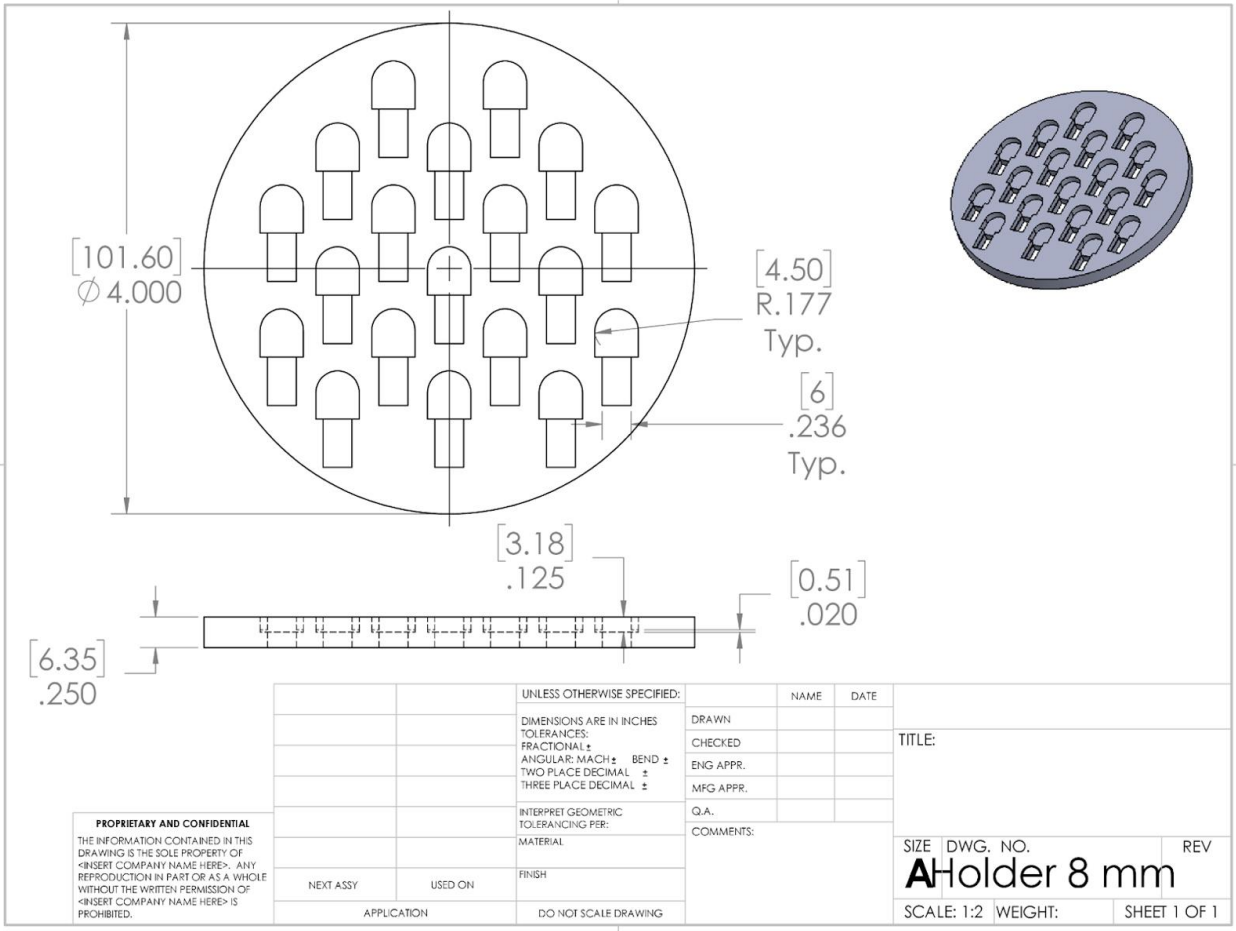

Figure A. 1 Dimensions and 3D rendering of fixture design produced in SolidWorks

Samples are required to be 8mm in diameter and coated on both sides for the radiolabeling experiments because they are immersed in solutions in small cups. The spin-cast polymers (PVDF and PVDF-HFP) required gold substrates for optimal polymer film quality and stability, with gold adhesion aided by a titanium adhesion layer. The metals were deposited using electron-beam evaporation to provide smooth, uniform coverage. This fixture was designed to fit into the planetary fixture of an electron beam evaporator from CHA Industries housed at the Washington Nanofabrication Facility (Seattle, WA), originally meant to hold 100 mm wafers.

This holder's design allows for easy placement of 8 mm glass coverslips on the flat indents of the holder, then sliding into the rectangular keyhole slots, which prevents them from falling. After coating the first side, the holder can be flipped over, and the second side of the samples coated. This method allows for maximal surface coverage of the titanium adhesion layer (5 nm) and gold (100 nm) without risking damage to the first side coated.

APPENDIX B - PLATELET ANTIBODY TITRATION

In order to confidently visualize platelets adhered onto the materials tested in the future, a combination of scanning electron and fluorescence microscopy must be used. The former provides the resolution needed to distinguish platelet morphologies, while the latter (with an appropriate antibody) provides confirmation of whether or not surfaces that appear bare are truly bare. This is important to check due to the ability of platelets to fully spread and become very difficult to visually distinguish from the surface. A calcium-dependent antibody that targets the GpIIb/IIIa site, PerCP-Cy™5.5 Mouse Anti-Human CD41a (BD Biosciences, #340931), was titrated to obtain the appropriate concentration for use in fluorescence microscopy. In doing so, a protocol for the fluorescent component of the experiment was also established. Based upon the recommendations of Dr. Ilya Reviakine and Dr. Mei Speer, antibody concentrations of 0.25, 0.5, and 0.75 μg/mL were chosen. Table B.1 explains the experimental setup of the titration. Based on past platelet adhesion experiments, which are beyond the scope of this thesis, and availability of materials, skived PTFE was chosen as a representative fluoropolymer material, on which a low number of platelets were expected to adhere. Collagen coated glass coverslips were chosen as a positive material, on which a high number of platelets were expected to adhere. The positive control and representative fluoropolymer samples were both treated as follows.

Samples were rinsed twice with calcium-containing PBS (PBS+Ca), then preadsorbed with a binary protein solution equivalent to that used in the radiolabeling experiments (but in PBS+Ca) for 2 hrs. Following two washes with PBS+Ca, the samples were then incubated for 1.5 hrs with platelets in Tyrodes buffer with 0.125 μL/mL prostacyclin (Pgl2) and 4μL/mL apyrase. Following another two washes with PBS+Ca, the samples were then incubated for 40 min with the antibody

at room temperature in the dark. Then, after three washes with PBS+Ca, the samples were then fixed with half-strength Karnovsky's fixative overnight at 4°C in the dark, washed another three times with PBS+Ca, and stored in the dark at 4°C until imaging. Antibody washes consisted of 5-minute soaks in the PBS+Ca.

Negative controls were included for both PTFE and collagen surfaces, wherein only proteins and antibody were added to the surface (no platelets) to rule out nonspecific binding. Additionally, some PTFE and collagen surfaces were exposed to only proteins and platelets (no antibody) as autofluorescence controls. Labeling was found to be equally intense across all concentrations tested, so 0.125 µL/mL is recommended for future experiments. Additionally, controls showed no nonspecific binding or autofluorescence, suggesting that platelet adhesion fluorescence experiments should be done according to the protocol described above.

Table B. 1 Experimental setup of GBIIb/IIIa antibody titration.

	# Platelets Expected		
	Few	**Many**	**None**
Antibody Concentration	**Representative material**	**+ control**	**- control**
0.25 ug/ml	2 PTFE	2 collagen	1 PTFE 1 collagen
0.5 ug/ml	2 PTFE	2 collagen	1 PTFE 1 collagen
0.75 ug/ml	2 PTFE	2 collagen	1 PTFE 1 collagen

APPENDIX C - PLATELET ADHESION ASSAY

Prostacyclin Optimization

Given the high sensitivity of platelets to handling conditions, a detailed protocol for visualizing platelets adhered on surfaces is included below. Solution formulas may be found in the corresponding protocol file in the group database. To minimize platelets activation from handling during their isolation from blood, the enzymes apyrase and prostacyclin (Pgl2) are added in the beginning then rinsed away prior to platelet deposition on surfaces. These enzymes help to maintain platelet shape and inactivation, but Pgl2 in particular can interfere with platelet-surface interactions, so the concentration was optimized using skived PTFE. Figure C.1 shows the results. By performing the platelet adhesion assay protocol detailed below with varying concentrations of Pgl2, it was determined that 0.25 µL/mL or less would not affect platelet response. To be safe, 0.125 µL/mL Pgl2 is recommended.

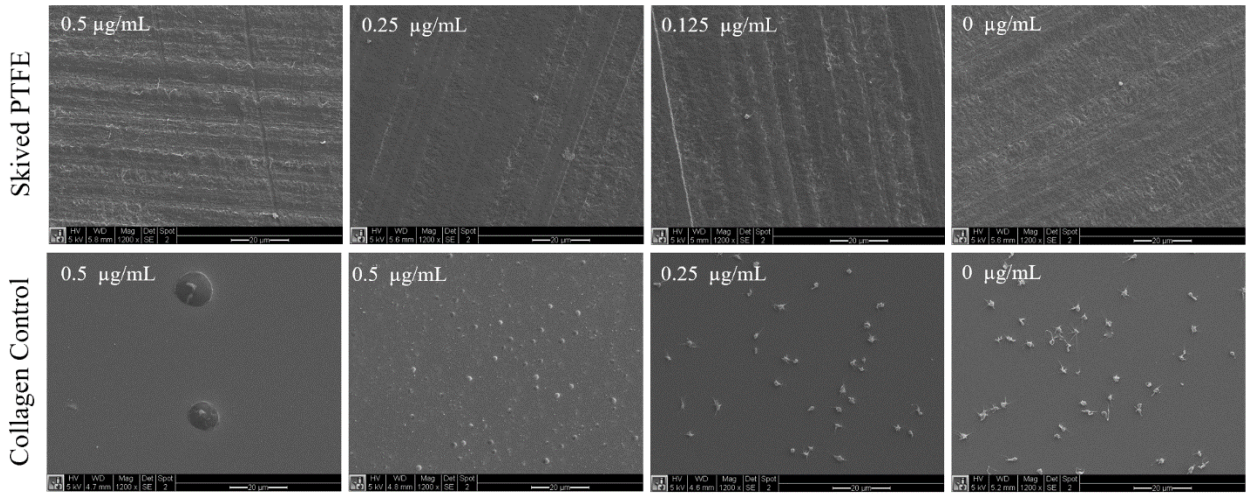

Figure C. 1 Prostacyclin optimization results, with concentrations listed per image. Scale bars = 20 µm.

Blood Processing & Platelet Preparation Protocol

*Note that platelets should be processed in 50mL conical tubes with **gentle** handling at every step. Also, after equilibration, all Tyrodes Buffer solutions (e.g. TyPR, TA) should be held in a 5% CO_2 cell culture incubator during spins. The following steps will become unnecessary if pooled platelet rich plasma is obtained from a blood bank. Nevertheless, if using blood from recruited human donors, take the following steps:*

a. Blood is drawn by a trained phlebotomist at UWMC in ACD (Acid Citrate Dextrose anticoagulant solution), handled at RT, and held in plastic only. You will need 2 blood vials per 10 samples/wells in a 12-well plate. Each ACD tube contains 10mL of fresh whole blood, which will be separated via the following steps into 2mL of platelets per well. If working with >2 vials, split total volume in half (two separate 50mL tubes) and proceed with steps below in parallel. It is most efficient to do steps C.a and C.b first and prep blood while waiting.
b. FIRST SPIN: Using a plastic pipet, transfer blood from ACD tube to 50mL conical tube. Centrifuge at 200G for 20 minutes, with 0 brake, ramping up speed in 2 increments. Set the timer when the speed is 200G. This separates the platelet-rich plasma (PRP). Always handle gently and avoid creating bubbles or aspirating red blood cells. When spinning any human blood you must use bucket caps on the rotor buckets and you must load and unload the rotor buckets/caps inside the biosafety cabinet. Transfer supernatant (~ 7mL PRP) to new 50mL conical tube. Be very careful to not disturb the interface between the layers (buffy coat).
c. SECOND SPIN: Centrifuge the PRP at 100G for 10 minutes, with 0 brake. Set timer when speed is 100G. This spin removes contaminating RBCs and WBCs. Prepare 1X TyPR by adding apyrase and PGI2. Carefully draw off only the plasma supernatant (~6.5mL) without

disturbing the pellet, and transfer solution to fresh 50mL conical tube, being very careful to not disturb the contaminated pellet. Add a volume of equilibrated TyPR equal to the amount harvested and gently invert tube 2-3x to mix. Discard the small loose pellet.

d. FINAL SPIN: Centrifuge diluted PRP at 2000G for 15min, with 0 brake. Ramp up speed in 3 increments (600, 1300, 2000G). This spin will pellet the platelets and provide a light platelet rinse. While waiting for centrifuge, prepare 2 x three 1.5mL Eppendorf tubes labeled A, B, C with a 1:1 Trypan Blue (T.blu) to PBS volume ratio according to dilution formulas in step B.e.i below. Specifically, make a separate tube with 2mL of 1:1 PBS/T.blu, then use in dilutions. Tube C is a back-up in case B has too-dense platelets and further dilution is needed.

e. RESUSPEND: Without disturbing the pellet, transfer most (~12mL or all but 1mL) of the supernatant to new tube and set aside (just in case). Gently rinse the remaining pellet with 3mL TyPR and aspirate, leaving behind approximately 0.5-1.0mL of TyPR. Gently tap the bottom of the tube with the platelet pellet. The pellet should dissolve and melt into the leftover TyPR. Add 1mL TyB buffer and gently tap the bottom of the tube to dilute melted pellet. After pellet is completely melted, add additional TyB buffer so final volume is 3mL per ACD tube.

f. Count platelets at 1:500 dilution, made as follows:

    1. Use platelet resuspension to make the following dilutions in the labeled Eppendorf tubes, mixing thoroughly. Aliquot 2 x 25uL platelet suspension into Dilution A, then place bulk platelet suspension in incubator.

A dilution	B dilution
25uL platelets	25uL "A" dilution
475uL 1X PBS/T.blu	600uL 1X PBS/T.blu
[final]=1:20	[final]=1:500

2. Count platelets in both B dilutions using the designated BSL-2 hemocytometer: clean hemocytometer and coverslip with ethanol, load dilution B first, use a new tip for each side. The dilution factor is 500 if dilution B is used, 20 is dilution A is used.
3. Calculate the volume of platelet suspension needed so that platelets are 10^8/mL. Your final total volume will be 2 mL / sample. Remember to clean and disinfect hemocytometer after use. Wipe down with kim wipe then spray with Cavicide and allow to sit 5 minutes.

g. Using 1X TA buffer, adjust liquid volume so [final] = 1 x 10^8/mL platelets. First mix the $CaCl_2$ and $MgCl_2$ well with TyB, then add platelet suspension and swirl tube to mix. Triturate twice with plastic pipet before adding suspended platelets to your sample wells.

Sample Calculation: Need 36mL platelet suspension, use 360uL each of $CaCl_2$ and $MgCl_2$. Use [36 – 0.72mL – volume cell suspension] mL of TA.

Platelet Adhesion Assay, Fixing, and SEM Preparation

1. Rinse samples 2X with 1X PBS+Ca. If a sample does not remain submerged, use a polystyrene weight. Only weigh down one edge of the sample with the weight, do not place weight directly over center.
2. Preadsorb each well with 2 mL of 1% human plasma or protein solution in 1X PBS+Ca for 2hrs @ 37°C and 5% CO_2 in BSL-2 incubator (top right), then aspirate.

3. Rinse 2X with 1X PBS+Ca to remove unbound proteins.
4. Add 2 mL of platelets/1X TA buffer mix from step B.g to each sample.
5. Place in 37°C and 5% CO_2 BSL-2 incubator (top right) for 90 minutes. After platelets are in incubator, gently stir them in a "+" formation (up-down, then left-right) to evenly disperse platelets.
6. Rinse 6X with 1X PBS+Ca to remove non-adherent platelets.
7. Fix samples. Note: All the following steps are done in a fume hood over an absorbent pad, collect all rinses in suction flask and dispose of as labeled hazardous waste.
    1. Fix samples 2 hrs at RT or overnight at 4°C in 2 mL Karnovsky's solution per well. Parafilm plate and place in dated/labeled secondary container. If leaving overnight, allow the plate and contents to warm up to room temperature before continuing with next ethanol dehydration steps.
    2. Rinse using 2.0 mL CaCo rinse per well, 3 x 10 min at RT (room temperature)
    3. Stain using 1.5 mL OsO_4 stain per well, 30 min at RT
    4. Rinse using 2.0 mL CaCo rinse per well, 3 x 10 min at RT
    5. Rinse in 50% ethanol, 2 x 5min at RT
    6. The 1st and 2nd 50% ethanol rinse is collected as hazardous waste. Empty the waste flask, rinse 2X with 10mLs 50% ethanol and collect that rinse as hazardous waste before collecting the 70% ethanol rinse. Beginning with the 70% ethanol rinse you will collect the washes as ethanol only waste ([final]=85%).
    7. Rinse in 70% ethanol, 1 x 15 min at RT (stop here if you're done for the day, leave at 4°C overnight). This is the recommended stopping point to minimize duration of the next

day's prep. If you have too many samples for one critical point drying (CPD) run, consider leaving one plate in 70% ethanol overnight and doing CPD the next day.

8. Rinse in 80% ethanol, 1 x 15 min at RT
9. Rinse in 90% ethanol, 1 x 15 min at RT
10. Rinse in 100% ethanol, 1 x 15 min at RT
11. Change 100% ethanol rinse, parafilm the plate underneath its cover, and transport to MolES for CPD in a secondary container. Take care that the samples remain under 100% ethanol during transport and when transferred to ethanol-filled CPD chamber.

8. Perform CPD, then mount samples on SEM stubs and sputter coat with 4 nm Au/Pd. Store the samples in a sealed container with a desiccator packet.
9. Image samples using an SEM in secondary electron mode, collecting images at 125pA (on the FEI XL-30 FESEM at the Molecular Analysis Facility, this corresponds to a 5 kV current and spot size 2.